INSTITUTE OF PHYSICS PUBLISHING REPORTS ON PROGRESS IN PHYSICS

Rep. Prog. Phys. **66** (2003) 1095–1144 PII: S0034-4885(03)18707-6

Developments in large gamma-ray detector arrays

I Y Lee, M A Deleplanque and K Vetter[1]

Nuclear Science Division, Lawrence Berkeley National Laboratory, Berkeley, CA, 94720, USA

Received 17 February 2003
Published 26 May 2003
Online at stacks.iop.org/RoPP/66/1095

Abstract

Gamma-ray spectroscopy was revolutionized with the introduction of high energy-resolution semiconductor germanium (Ge) detectors in the early 1960s. This led to the large increase in sensitivity realized by today's arrays of Compton-suppressed Ge detectors. A still larger increase in sensitivity is expected by implementing the new concept of tracking. A tracking array consists of highly segmented Ge detectors (that can cover the full 4π solid-angle) in which γ rays will be identified by measuring and tracking every γ-ray interaction. This article reviews the physics motivation for such detectors and the development of the new technologies involved. The concept of tracking is explained using the example of a proposed array called γ-ray energy tracking array (GRETA).

[1] Current address: Glenn Seaborg Institute, Lawrence Livermore National Laboratory, Livermore, CA, 94550, USA.

0034-4885/03/071095+50$90.00

Contents

1. Introduction

The energies of electromagnetic radiations span eighteen orders of magnitude, from $\sim 10^{-6}$ eV used in radio and telecommunications, to $\sim 10^{6}$ MeV produced in cataclysmic events in galactic nuclei. Gamma rays refer to the upper part of the range, above about 0.1 MeV. At the highest part of this range, the higher energy γ rays (above 20 MeV) are detected with very different techniques from those reviewed in this article, Pb calorimeters or atmospheric air showers associated with Cherenkov light detectors. We shall focus here on the detection of γ rays with energies ranging from 0.1 to $\sim$20 MeV which is the natural range for γ rays emitted by nuclei. Germanium (Ge) semi-conductor detectors are most commonly used in this energy range when high energy-resolution is needed. Unprecedented development of arrays of Ge detectors has occurred in the last two decades and it has been driven both by physics (largely nuclear physics) and by technological advances. The purpose of this article is to review the development of high-resolution γ-ray detectors together with some of the nuclear physics motivation.

Gamma rays are emitted in nuclear processes during radioactive decay or in nuclear reactions. Detection of these γ rays gives basic information on the nuclear energy levels: their energy and intensity determine the position of the levels; the γ-ray emission times measure the lifetime of levels which, in some cases, can give deformation parameters; their polarization gives the parity of levels; and their angular distributions and correlations provide information about spins, magnetic moments, and static quadrupole moments, among other things. In the last 10–15 years, large improvements in efficiency and sensitivity of high energy-resolution detectors have led to important discoveries in nuclear structure.

Generally, nuclear reactions occur when an energetic beam of nuclei impinges on fixed target nuclei. In the beam-energy range used in nuclear structure studies (a few megaelectronvolts per nucleon), the two nuclei may fuse to form a 'compound nucleus' which can have a range of excitation energies and angular momenta. Typically, these nuclei de-excite by emitting a few nucleons (which remove much of the energy) and then by γ-ray cascades which remove most of the angular-momentum. Because the reactions introduce up to nearly $90\hbar$ of angular-momentum and the dominant multipolarities of this γ radiation are dipole or quadrupole (removing only 1 or $2\hbar$ each), many γ rays will be emitted in a cascade from a high-angular-momentum event. It is the study of these γ rays that gives the information on the structure of the nucleus. Based on this picture, almost any kind of nuclear physics study involving γ rays requires selecting particular cascades of γ rays from a high background of unwanted γ rays. These unwanted γ rays are of two kinds: (i) the γ rays with partial-energy deposited in the detector, which do not contain any useful information; (ii) the many other cascades produced in reactions that are not of interest. This selection is typically made by constructing multi-dimensional spectra of time-correlated (coincident) γ rays which compose a (partial) decay cascade in the nuclear reaction. Multi-dimensional spectra are essential as they provide a larger space to isolate the various cascades.

In order to isolate the interesting cascades, several requirements must be met.

(1) Two γ rays close in energy should be distinguishable. This means that the peak associated with γ rays of a given energy in a spectrum should be as narrow as possible. We refer to this characteristic as a high energy-resolution. This is fulfilled in Ge semiconductors because of the small band gap between the valence band and the conduction band. Typically, the width of a 1 MeV γ-ray peak is around 2 keV (0.2%).

(2) The detection of full-energy peaks should be as efficient as possible, i.e. we need a high full-energy efficiency. This requires large Ge crystals. The typical large detectors are cylinders approximately 7 cm in diameter and 8 cm in length (7×8). Still only 20% of incident 1 MeV γ rays deposit their full-energy in such a detector. The incident γ ray

traverses the detector without interaction 10% of the time and 70% of the time the γ ray interacts but a Compton-scattered γ ray escapes the detector before it interacts again. (Typically a 1 MeV γ ray that deposits its full-energy in one detector has interacted four times in that detector.) This property is referred to as a 22% peak-to-total ratio (0.2/0.9).

(3) Since there are often many γ rays (e.g. 20–30) emitted in each event, we need in principle to detect each one separately in each detector, otherwise we lose the single γ ray energy information. Therefore, a detector system should consist of an array of many detectors and it is said to have a high granularity.

(4) To eliminate the partial-energy events, the Ge detector is surrounded by a Compton suppressor, a low-resolution detector which detects very efficiently the scattered γ rays that escape, and gives a signal vetoing the recording of the energy deposited in the Ge detector, thus increasing the peak-to-total ratio. For the last twenty years, the best performance was obtained by using large arrays of Compton-suppressed Ge detectors. One of the two largest present arrays, Gammasphere [1], consists of 110 such detector–suppressor elements.

(5) Since we accumulate γ rays from many events in a multi-dimensional array, we need to keep the time correlation of the coincident γ rays within a cascade that constitutes an event. This is done by extracting a time signal from each detector and then using fast electronics to correlate them. Typically, a time resolution of 5–10 ns is achieved.

Recently, it was realized that more could be gained by adding back the Compton scattered γ ray rather than using it to suppress the γ ray. The first step was the use of composite Ge detectors where one could add the time-correlated signal from an adjacent Ge detector. But in the last 7–8 years, the concept of tracking detectors has been developed and it has been shown that, in certain applications, a factor of at least 1000 in sensitivity over previous arrays could be gained by using an array of tracking detectors. In effect, such an array is equivalent to a set of many ($\sim$3600) small detectors, each detecting one γ-ray interaction, all of which are used to reconstruct the incident γ rays with much better efficiency than before.

In addition to developing new and more efficient detectors or arrays, major developments in electronics and computer systems have been necessary to handle the vast increase in data processing. This means not only fast and reliable 'miniaturized' electronics but also a lot of computer storage space to record and process the data. Both have evolved rapidly in recent years and will be reviewed in the context of the γ-ray detector developments.

2. Evolution of gamma-ray detectors: historical perspective

Gamma-ray detection is based on the effect of a γ ray interacting with matter [2, 3]. For our purposes there are only three important types of interaction of a γ ray with matter. These are called (I) the photoelectric effect, (II) the Compton effect and (III) the pair-production effect. The characteristics of these effects are important in detector design and we will review them briefly.

2.1. Interaction of γ radiation with matter

At low γ-ray energies ($E_\gamma < 0.2$ MeV), the photoelectric effect dominates (see figure 1). In this process, the γ ray is absorbed and the energy is used to eject a bound electron from an atom in the detector material, ionizing the atom. The electron cannot be free because a third body must be present to ensure momentum conservation. Subsequently, the vacancy is filled and the emitted x rays are absorbed (through subsequent photoelectric effects) and the ejected electron is stopped through collisions with other loosely bound electrons. The net effect is the

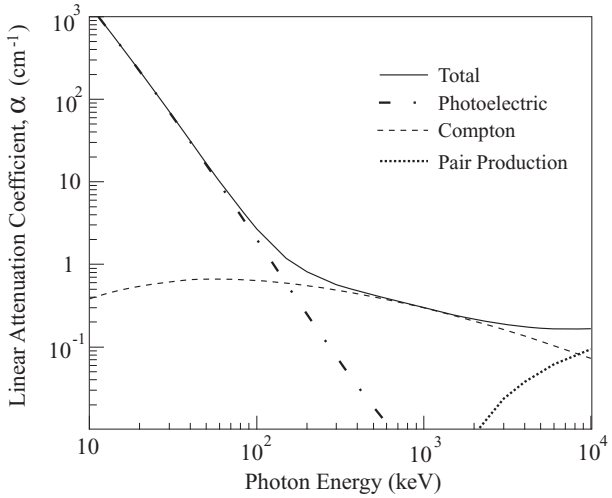

Figure 1. Linear γ-ray attenuation coefficients (proportional to the cross section) for photoelectric, Compton and pair-production interactions in Ge material as a function of γ-ray energy. The total absorption coefficient is also shown.

production of primary ion–electron pairs whose number is proportional to the γ-ray energy. The cross section for this process is roughly proportional to Z^n/E_γ^3, with n between 4 and 5, emphasizing the need for high-atomic number (Z) detector materials.

In the medium-energy range ($0.2 < E_\gamma < 5\,\mathrm{MeV}$), the predominant interaction is Compton scattering; i.e. the elastic collision of a photon on an outer electron (of the absorbing material) considered as free. Thus, the incident photon of energy E_γ scatters into another photon of smaller energy E'_γ at an angle θ to the incident direction and the rest of the energy is carried by the electron. The energy of the scattered photon depends on the scattering angle θ:

$$E'_\gamma = \frac{E_\gamma}{1 + (E_\gamma/m_0c^2)(1 - \cos\theta)} \tag{1}$$

where m_0 is the mass of the electron ($m_0c^2 = 0.511\,\mathrm{MeV}$). The angular distribution of the scattered photon depends on E_γ and is given by the Klein–Nishina formula (see [4]): the probability for forward scattering increases with the γ-ray energy. The scattered γ ray can either: (i) interact again in the same detector through a photoelectric effect or another Compton scattering and the process may continue until all the γ-ray energy is absorbed in the detector; or (ii) it may escape the detector and part of the incident energy is lost. Thus, an incident γ ray that Compton scatters out of the detector produces a signal with any energy up to a certain maximum (called the Compton edge) deduced from the above formula (at $\theta = 180^\circ$) and therefore does not give the energy information of the incident γ ray (see figure 10-1 in [5]). The cross section for Compton scattering is proportional to Z (i.e. to the number of free electrons).

At higher energies ($E_\gamma > 5\,\mathrm{MeV}$) the pair-production process dominates (its threshold is 1.022 MeV, or twice the electron rest mass). A photon produces an electron–positron pair in the electric field of a nucleus in the detector material. The energy in excess of 1.022 MeV goes into kinetic energy of the electron and the positron. The positron subsequently annihilates after slowing down in the detector material and this creates two 0.511 MeV photons that are emitted back to back in angle. One or two of these photons may escape the detector, leaving in the detector an energy $E_\gamma - 0.511\,\mathrm{MeV}$ (which gives rise to the single-escape peak in a spectrum)

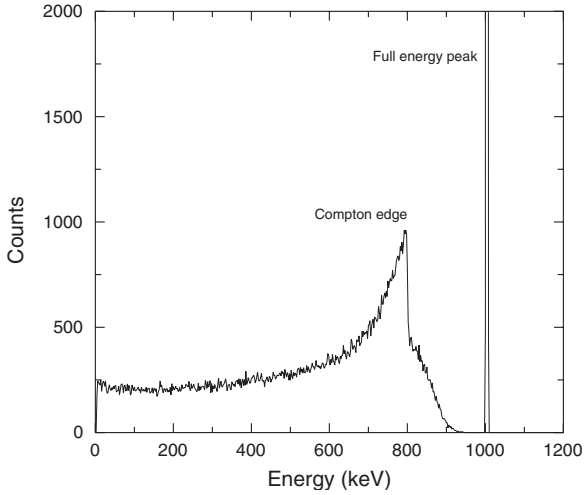

Figure 2. Response (distribution of pulse-heights) of a Ge detector to a monoenergetic 1 MeV γ-ray source. The height of the full-energy peak is off-scale in order to show the Compton distribution.

or $E_\gamma - 1.022\,\mathrm{MeV}$ (double-escape peak). The cross section for this process (see [3]) is approximately proportional to Z^2.

2.2. Detector response

Figure 2 shows the response of a typical γ-ray detector, (here a large Ge detector, 10 cm diameter $\times$ 9 cm long) to a monoenergetic γ-ray source in the simplest case where the γ-ray energy is below the pair-creation threshold. This spectrum is the distribution of pulse-heights obtained at the output of the detector from identical γ rays that interacted in the Ge crystal. The full-energy peak corresponds to events where the incident γ ray was fully absorbed in the detector through a photoelectric effect or through several Compton interactions followed by a photoelectric effect. Below the full-energy peak, the lower energy continuum is due to escaped Compton events. In an event in which the first scattered photon escapes the crystal, the energy in the detector is less than the Compton edge. Multiple Compton events where the last scattered photon finally escapes give a signal between the Compton edge and the full-energy peak. From this spectrum, one can define the two most important characteristics of a detector. (1) Energy-resolution; the energy-resolution $\delta E_\gamma / E_\gamma$ of the detector is defined as the full-width at half-maximum (FWHM) of the full-energy peak divided by the mean pulse-height of the full-energy peak (therefore expressed as a percentage). (2) Peak-to-total ratio (P/T); this ratio expresses the fraction of useful γ-ray counts in the spectrum. It is the ratio of the area of the full-energy peak to the total spectrum area.

2.3. The semiconductor Ge detectors

Germanium semiconductor detectors were first introduced in 1962 (see [6]) and are now the detectors of choice for high energy-resolution γ-ray studies. These detectors directly collect the charges produced by the ionization of the semiconductor material. One electron–hole pair is produced on the average for every 3 eV absorbed from the radiation. (This results in approximately a factor of hundred more charge than can be obtained for a typical scintillator material, e.g. NaI(Tl).) These pairs drift under an external electric field to the electrodes where

they generate the pulse. The high number of information carriers leads to a small percentage fluctuation and this is the reason for the high energy-resolution (of order 0.2% for a 1 MeV γ ray) of Ge detectors.

Semiconductors used in detectors are single crystals and the periodic lattice generates electron bands (allowed levels for the electrons in the solid) which are separated by regions of forbidden energy or band gaps. The electrons that form the covalent bonds are bound to the crystal and completely fill one band which is called the valence band. The next higher band is called the conduction band and when it is partially filled, as in metals, the material is a conductor. When the two ends of a piece of conductor are connected to different potentials, a current flows that would mask a current generated by an ionizing radiation. In an insulator or a semiconductor, the conduction band is empty and only the thermal excitation generates a current in the absence of ionizing radiation. This is called the bulk leakage current and it is greater in a semiconductor (where the band gap is smaller, $\sim$1 eV) than in an insulator (where the band gap is $\sim$5 eV). Both the larger band gap and the charge carrier transport properties eliminate insulators as possible detector materials. Insulators tend to trap the charges that are created by the γ rays and therefore the incomplete charge collection gives a degraded signal that is not proportional to the γ-ray energy. In contrast, charge carriers in semiconductors have a high mobility. It turns out that only two single-element semiconductor materials, namely silicon (Si) and germanium (Ge), (and a number of compound materials, see section 3.5.2) give a signal that is high enough above the noise (reasonably large band gap), is proportional to the energy deposited in the crystal (little trapping), and have a good energy-resolution (reasonably small band gap).

However, the detector cannot simply consist of the semiconductor material and two electrodes because there are inherent impurities in these materials. Both Si and Ge have a valence 4 and when an impurity of valence 3 (acceptor) or 5 (donor) exists in the crystal, it lowers the energy necessary to create electron–hole pairs and this tends to create too much noise. The Ge crystal with acceptor impurities is called p-type (Ge) material and the same with donor impurities is called n-type (Ge) material. The solution (see [5, 7, 8]) is to create a p–n junction at one electrode and to polarize it so that no current passes through when there is no ionizing radiation (this is called reverse biasing or using non-injecting or blocking electrodes). This creates a region called the depletion layer where few charge carriers remain, resembling a pure semiconductor. With a sufficient voltage, the electric field can create a large enough depleted volume to make a viable detector (see section 3.1.1).

2.3.1. The Ge(Li) detectors. The first semiconductor detectors were very small because the depletion layer could only be made very thin (a few millimetres) before the high electric field applied would break down the detector. In 1960, it was shown [9] that much thicker depletion layers could be obtained by compensating the excess impurity in the p-type material. This could be achieved by drifting at somewhat high temperature some donor in that contact, largely neutralizing the existing impurities. The reason for this 'breakthrough' is that the donor (interstitial) small ions of Li can be drifted easily by an electric field and that the donor impurities compensate 'exactly' the acceptor ones. With such a process, detectors of thickness up to 20 mm could be made, greatly improving the detection efficiency. After the drifting process, the detector must be kept cold (generally at the liquid nitrogen temperature of 77 K) to prevent the lithium from diffusing in the crystal and destroying the compensation.

2.3.2. The high-purity Ge (HPGe) detectors. A step forward was achieved when higher purity Ge material could be fabricated [10,11], with impurity concentration of 10^{10} atoms cm^{-3}

instead of 10^{13} atoms cm^{-3}, eliminating the need for Li compensation. This means that the material has a higher resistivity which is proportional to the square of the depletion layer's thickness. This paved the way for the manufacture of larger and much more efficient detectors. More details on the properties of semiconductor detectors will be given in the next section.

2.4. Gamma-ray detector arrays

A system with more than one detector allowed γ–γ coincidence experiments where two γ rays are identified through time correlation as belonging to the same cascade from one event. Fairly complicated level schemes could then be constructed, leading to much more refined studies of nuclear structure.

The next big step in γ-ray detection occurred in 1980s when the first arrays of multiple Ge detectors were assembled. There were two factors that greatly increased the power of such detection systems. First, the number, N, of Ge detectors used increased the coincidence efficiency which is proportional to $(N\epsilon)^f$, where f is the number of γ rays detected (f is called the fold number) and ϵ is the efficiency of one detector. Second, the use of Compton-suppressed Ge detectors increased the peak-to-total ratio significantly (typically from ∼20% to ∼50%) and therefore reduced the background of γ rays that do not carry energy information. These developments have culminated in large arrays with nearly 4π solid-angle coverage and involving approximately 100 detectors. The two largest arrays today are Gammasphere [1] in the US and Euroball [12, 13] in Europe.

2.5. Towards the ultimate array

Ideally, one would like to detect every γ ray emitted in an event and know its energy, emission angle and time, each with good resolution. One could then do an event-by-event analysis, and know all the states a nucleus is decaying through as it de-excites. This would give a much more detailed knowledge of the nuclear structure. In practice, this cannot be done because the Ge detectors are not 100% efficient; they cannot be made long enough, and there are dead layers and lost space between the detectors. Also the granularity needs to be high to allow complete separation of each individual γ ray.

The newest idea is to use a 'shell' of many (∼100) highly segmented Ge detectors and to 'recognize' when partial energies come from a single incident γ ray by tracking each interaction in each detector. This is far more efficient than using Compton suppressors. However, this latest advance is still in the research and development stage. We will end this review by describing such a system that we are currently developing called the gamma ray energy tracking array (GRETA).

3. Properties of Ge semiconductor detectors

3.1. Description of a HPGe detector

In this section, we will describe HPGe detectors. A HPGe detector is a p–n junction of extremely high-purity material (i.e. with an impurity concentration as low as ∼10^{10} atoms cm^{-3}).

3.1.1. Basic principle. Figure 3 shows the configuration of a HPGe planar detector. In this example, an n-type material is used. A p–n junction is formed by implanting boron onto the (left) surface of the Ge which has been lapped. This surface then contains highly doped p-type

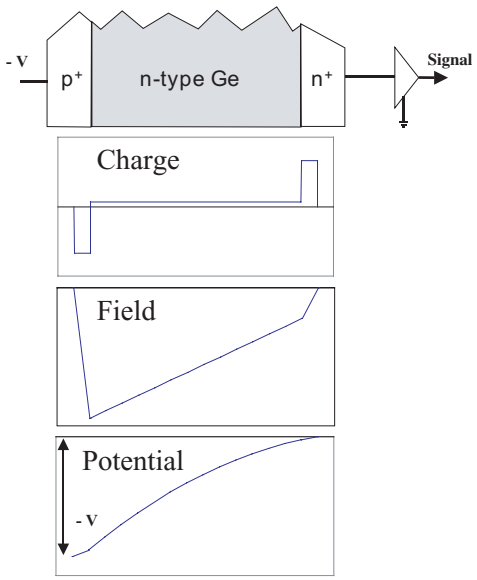

Figure 3. From top to bottom: configuration of an n-type intrinsic germanium planar detector; charge distribution for the fully depleted detector; electric field and electric potential profiles along the detector.

material (noted by p+). On the right surface, a layer of highly doped n-type material (n+) is created by diffusing Li over a very thin region of the material. At the p–n junction (left edge), a charge carrier diffusion occurs (electrons into the p+ layer and holes into the bulk n-type material) because of abrupt density gradients. The overall effect is a net negative space charge of electrons in the p+ contact and a net positive space charge of filled donor sites in the n-type material, extending over a finite region near the junction called the depletion layer. This creates a potential difference called a contact potential which prevents further diffusion of electrons and holes. The sites in the thin depletion layer do not contribute to the conductivity, therefore the material in the depletion layer has a very high resistivity.

A reverse biasing of this structure (p–n junction, bulk n-type material, and n+ contact) consists of applying a negative voltage on the p+ side as indicated in figure 3. The p+ contact (i.e. the contact on the p–n junction side) is called the rectifying contact. Practically, all the applied voltage appears at the edges of the depletion region because of its very high resistivity as compared with the adjacent regions. However, since the reverse biasing increases the potential difference above the contact potential, application of the Poisson equation implies that the space charge both increases and extends further. (The Poisson equation reads $\nabla^2\varphi = -\rho/\epsilon_m$, where φ is the potential at any point, ρ is the net charge density, and ϵ_m is the dielectric constant of the material.) When sufficient voltage is applied, the depletion layer extends over the full length of the n-type material and the resulting space charge is shown in figure 3. As mentioned before, the region of the depletion layer, which constitutes the active volume of the detector, has a very high resistivity and therefore its leakage current is very small. When a γ ray interacts in the active volume, it creates electrons which are collected on the n+ contact, while the holes are collected on the p+ contact, and the current that occurs as the electrons and holes move toward the electrodes, once integrated, constitutes the γ-ray energy signal.

In practice, one increases the applied voltage beyond the value necessary for full depletion by a quantity called the overvoltage in order to increase the mobility of the electrons and holes

and ensure that the total charge created by the γ ray is collected before it is trapped in the material or recombines. The operating electric field and electric potential are shown in figure 3 for an n-type HPGe planar detector. Note that the amount of overvoltage is limited by the purity of the material since a lower resistivity would lead to a breakdown of the detector at a lower voltage.

3.1.2. Shape. Since the depth of the depletion layer is limited by the material itself, it is obvious that a co-axial configuration will lead to a larger active volume than a planar configuration. Figure 4 shows a schematic drawing of an n-type co-axial HPGe detector. In such a closed-end detector, a cylindrical hole is drilled along the central axis of the detector for the n+ Li-diffused contact, whose thickness is typically 600 μm. This hole does not reach the other end of the detector. The outer surface (except the flat face with the hole opening) is used as the implanted boron p+ contact which has a typical thickness of 0.3 μm. When a γ ray interaction occurs, the electrons move toward the inner electrode and the holes toward the outer electrode. The surface of the closed-end is usually the entrance window of the detector which is very thin. In such a detector, the electric field is not uniform over the active volume. The field lines are approximately radial except near the closed-end region.

3.1.3. n-type versus p-type. What determines the choice between n-type and p-type co-axial detectors is their sensitivity to radiation damage. In some of the most important applications using (many) large-volume HPGe detectors, such as for in-beam nuclear structure studies or for astrophysics, it is essential to maintain good energy-resolution when the detector is damaged by other radiation present, mostly fast-neutrons or high-energy protons. It turns out that manufacturers always locate the rectifying contact on the outer surface of a co-axial detector because the electric field is then highest at the outer surface where most of the detection volume is located. Radiation damage [14, 15] consists of hole traps which are produced when an energetic particle interacts with a Ge nucleus, imparting enough energy to the nucleus to dislocate many other Ge atoms in the lattice. This creates a disordered region which accumulates many electrons and electrostatically attracts and traps holes. One thus wants to minimize the distance travelled by holes, so they should travel to the outer surface. These two conditions require n-type detectors, and it has been found [16] that they are, indeed, more than an order of magnitude less sensitive to radiation damage than p-type detectors.

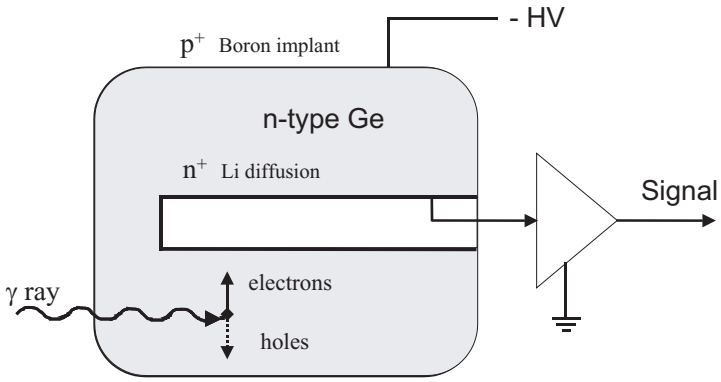

Figure 4. Configuration of an n-type intrinsic germanium closed-end co-axial detector.

Studies of temperature effects and bias effects on the performance of (n-type) radiation-damaged detectors [14] gives guidance on how best to operate them. The operating temperature should be as low as possible (below 85 K) since thermal electrons at higher temperature have enough energy to populate a hole trap, making it more negatively charged, and therefore a more efficient hole trap. The detectors should be kept under bias at all times since a detector with no bias has more negatively charged traps due to the presence of more free electrons in an undepleted n-type crystal.

Typically, with a fast-neutron (>1 MeV) flux of $\sim 5 \times 10^9$ n cm^{-2} [16, 17], the energy-resolution of a large n-type co-axial detector will start to show significant degradation. Hole traps can be removed by annealing the detector at approximately 100°C for a few days (under vacuum (10^{-6} mbar) to decrease the risk of surface contamination).

3.2. Energy-resolution, time resolution

The energy-resolution of a detector is usually defined as the FWHM of a monoenergetic full-energy peak (in the spectrum) divided by the value of this energy. The width of the peak originates from the random fluctuations that occur in the (statistical) charge creation and collection process and from various noise sources. The noise includes contributions from both the detector and its associated electronics. Typically, the FWHM is divided into two components, one of statistical origin and the other resulting from the noise in the system:

$$(\mathrm{FWHM})^2_{\mathrm{total}} = (\mathrm{FWHM})^2_{\mathrm{statistical}} + (\mathrm{FWHM})^2_{\mathrm{noise}} \tag{2}$$

3.2.1. Intrinsic energy-resolution. The intrinsic energy-resolution is the contribution to the energy-resolution which comes from the nature of the material and it is related to the charge creation statistics. In a Ge detector, the average ionization energy (i.e. energy expended on the average to create an electron–hole pair) is measured [18] to be 2.96 eV at 90 K whereas the band gap in Ge is ~0.7 eV. These differ because the pair-creation process involves complicated excitations in the crystal which are not fully understood. The creation of pairs is treated as a statistical process with random fluctuations calculated by assuming that the formation of each charge carrier obeys Poisson statistics. If there are N electron–hole pairs created on the average by a photon of energy E that is fully absorbed (i.e. $N = E/2.96$, where E is in units of electronvolts), the inherent fluctuation in the number of pairs is characterized by a standard deviation $\sigma = \sqrt{N}$. Then the response should be a Gaussian curve (because N is large) with a standard deviation $\sigma = \sqrt{N}$ and the FWHM in energy would be $2.35\sqrt{2.96E}$. In practice, there are correlations in the electron–hole formation process and the FWHM is reduced by a factor $\sqrt{F}$, where F is called the Fano factor. For Ge and Si material, F is approximately 0.12. Typical intrinsic Ge energy-resolutions are given in [19] for various energies. For example, at $E_\gamma = 1$ MeV, the $(\mathrm{FWHM})_{\mathrm{stat}}$ is 1.40 keV.

3.2.2. Noise contribution. The other important contribution to the width of an energy peak comes from the noise generated in the detector and in associated pulse processing electronics. However, energy-resolution is not the only consideration in performing a measurement. Typically, an experiment is performed at high counting rates in order to accumulate more counts. This entails shorter shaping times of the electronic pulses which tends to increase the noise. Thus compromises must be made to optimize the desired quality of the data. In the next paragraph, we will briefly review the basic features of the main electronics components in order to characterize the noise component. Other details will be given in section 5.

The basic elements of the electronic components for a pulse-shape analysis system are shown in figure 5. The electronic components transform the small current signal at the detector electrodes (figure 6, top) into a large voltage signal whose amplitude is proportional to the energy deposited by the radiation in the detector, and whose width is narrow enough to allow a high count rate without overlapping the signals. The most important component is the input stage of the preamplifier which is the field-effect transistor (FET) [20]. It is essential to minimize its noise since the signal is very small but, at the same time, the FET gain should be large enough to make noise sources in later stages negligible. In Ge detectors, the FET is commonly cooled to minimize the noise power which depends on the temperature. It is maintained at an optimum temperature of approximately 130 K where the noise is minimum [21]. This is slightly higher than the temperature of the detector itself (around 80 K) which would freeze out the main dopant of the FET. The pulse-shape at the output of the preamplifier is shown in figure 6 (middle) with a short rise-time corresponding to the charge collection time in the detector, an amplitude proportional to the charge accumulated at

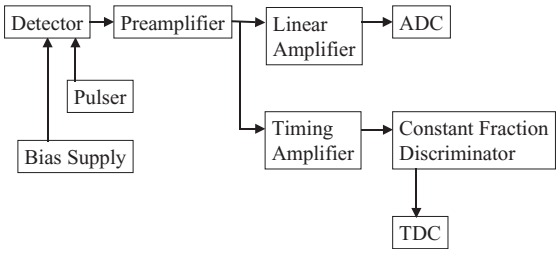

Figure 5. Basic electronic components for a pulse-height analysis.

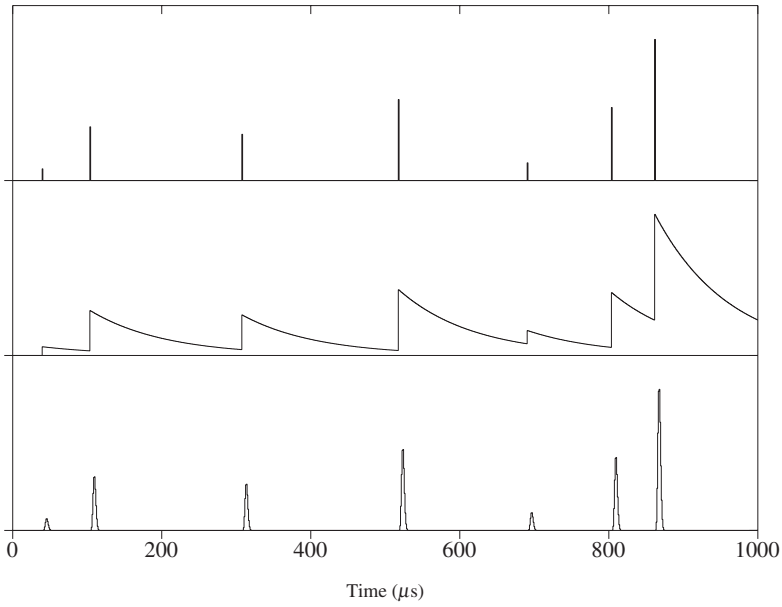

Figure 6. Top: current pulse produced by the detector (vertical arbitrary units). Middle: typical voltage output of a preamplifier as a function of time. The apparent amplitude varies due to pile-up of the pulses. Bottom: voltage output of the amplifier. By shaping the pulses, their true amplitude is recovered.

the electrodes and a comparatively long exponential decay time ($\sim$50 μs). This means that consecutive pulses might overlap.

The linear amplifier solves that problem by shaping the preamplifier signal so that it becomes shorter (figure 6, bottom) and at the same time, it filters out some noise. The simplest one is a CR differentiator followed by an RC integrator: the differentiator is a high-pass filter and will eliminate low-frequency noise, the integrator is a low-pass filter and will eliminate the high-frequency noise while the signal, which is confined to an intermediate narrower band, is unchanged. In practice, more complex combinations of differentiation and integration circuits are used. Baseline restorers [5, 19] further reduce baseline fluctuations. For example, the energy-resolution for a Gammasphere large (approximately 7 $\times$ 8) co-axial Ge detector is $\sim$2 keV for the 1.332 MeV γ ray from a ^{60}Co radioactive source with a shaping time of 16 μs.

3.2.3. Time resolution. In a typical nuclear structure experiment, an event is identified by the 'coincident' arrival time of the γ rays, typically within a few picoseconds (ps). A realistic time resolution of a few nanoseconds allows the separation of one event from another but does not give the time sequence of the γ rays within a cascade. The time resolution is defined as the FWHM of a distribution curve of the time interval between the detection, in two detectors, of two γ rays (which arrived nearly simultaneously).

The time associated with the detection of a γ ray is measured from the preamplifier signal. A signal with a fast rise-time is generated in a timing amplifier (see figure 5) and a time signal is then produced using a so-called constant fraction discriminator. It is widely used when there is a large range of signal amplitudes because the output signal is produced at a fixed time after the leading-edge of the pulse has reached a constant fraction of the pulse amplitude. Thus, this time is independent of the pulse amplitude provided. Uncertainties in the time measurement then come from noise in the electronic units as well as from signals having different shapes. Statistical fluctuations in the number of information carriers (e.g. distance travelled, impurities or field non-uniformities) will lead to fluctuations in the signal shape. A time resolution of a 4–5 ns is usually obtained for large HPGe detectors compared with a total rise-time of 200–300 ns.

3.3. Efficiency, peak-to-total ratio

3.3.1. Efficiency. The intrinsic full-energy peak efficiency ϵ_p of a detector is defined as the ratio of the area of the full-energy peak divided by the number of (monoenergetic) γ rays incident on the detector. One can also define an absolute full-energy efficiency ϵ_a which depends on the distance of the detector to the γ ray source and on the size of the detector, i.e. on the detector solid-angle Ω. This efficiency ϵ_a is the ratio of the area of the full-energy peak divided by the number of γ rays emitted by the source, i.e. $\epsilon_a = \epsilon_p(\Omega/4\pi)$. This definition assumes an isotropic emission by the source. Similar total efficiencies can be defined by using the total number of counts in the spectrum instead of the counts in the full-energy peak. For historical reasons, the full-energy peak efficiency is given [22] relative to that of a standard 7.5 cm diameter, 7.5 cm long cylindrical NaI(Tl) scintillator for the 1.33 MeV γ ray emitted by a ^{60}Co source located 25 cm from the detector (the NaI efficiency ϵ_a is 1.2×10^{-3}). Thus, for example, a typical Gammasphere HPGe detector has a 'relative efficiency' of 70%.

3.3.2. Detector size. The larger the active volume of a detector the larger is the chance of total absorption of the γ ray. However, larger detectors are not always desirable due to summing effects. In typical high-multiplicity experiments, where on the average 20 γ rays might be emitted per event, the chance that two γ rays hit the same detector can be high (e.g. for a

7 cm diameter detector at 25 cm from the source, the probability of 'summing' is 10%). This summing can be decreased by locating the detector farther from the source, but this causes a loss of efficiency. Given a typical γ-ray multiplicity of 20 there is therefore a balance between the diameter of a detector and its distance from the γ-ray source which optimizes the combination of full-energy efficiency and peak-to-total ratio. We will see in the next section that Compton suppression effectively selects fully absorbed γ rays, thereby increasing the P/T ratio.

3.4. Summary of properties

HPGe (n-type, co-axial) detectors are at present the best γ-ray detectors (in the energy range $\sim$0.1 to $\sim$10 MeV) due to: (i) the high energy-resolution of the semi-conductor Ge material; (ii) the high full-energy efficiency of large detectors; (iii) the large increase in peak-to-total ratio when augmented by Compton suppressors. For typical nuclear structure experiments with high γ-ray multiplicities, such detectors are arranged in large arrays. We will see in the next section that these three properties define the resolving power of such an array.

3.5. Comparison with other detectors

For completeness, we will mention other types of γ-ray detectors and briefly review their characteristics.

3.5.1. Si(Li) detectors. Because of the lower atomic number of silicon ($Z = 14$), the Si(Li) detectors are typically 50 times less efficient than Ge detectors for photoelectric absorption. Therefore, only low-energy γ rays (up to 200 keV) are detected with reasonable efficiency. However, the band gap is larger for silicon material than for Ge material ($\sim$1.1 eV for Si versus $\sim$ 0.7 eV for Ge), resulting in a smaller leakage current for Si detectors and therefore a better energy-resolution, provided they are cooled (see, e.g. [5], for more details on Si(Li) detectors).

3.5.2. Other semiconductor detectors. There are two main types of semiconductor detectors that use compound materials: CdZnTe (cadmium zinc telluride) and HgI_2 (mercuric iodide). Their main properties are: (i) high-atomic number components which result in a high efficiency; (ii) and relatively high band gap (1.5–2 eV) which reduces the leakage current and allows operation at room temperature. Unfortunately, these materials have low carrier mobility (especially hole mobility) and short lifetimes of carriers, which result in a poor energy-resolution and large detectors cannot be made. Nevertheless significant progress has been made recently in designing such detectors for some γ-ray applications [23].

3.5.3. Scintillators. In a scintillator, the electrons from the γ-ray interaction excite molecular levels in the crystal which return to their unperturbed state by emitting light, i.e. scintillating. A photocathode which sees the light emits photoelectrons which are then multiplied in a photomultiplier to give an electrical signal whose amplitude is proportional to the γ-ray energy.

There are four main types of scintillators used in different applications. Sodium iodide (NaI(Tl)) detectors have an efficiency similar to that of large Ge detectors. However, the energy required to emit a photoelectron is about 250 eV compared with 3 eV for Ge detectors. This results in a much worse energy-resolution (e.g. 6% instead of 0.2% at 662 keV), so they are not used when high-resolution is needed. However, very large NaI(Tl) detectors of various shapes can be manufactured, which makes them useful in other applications; for example efficient 4π detectors of total γ-ray energy emitted. Recently, portable scintillators have been

used for security purposes to detect the presence of illegal radiation. Barium fluoride (BaF_2) detectors have similar efficiency and slightly worse energy-resolution than NaI(Tl) detectors but the signal rise-time is much faster (0.5 ns instead of a few nanoseconds) and this permits the separation of γ rays and nuclear fragments based on differences in flight time. Experiments involving the detection of high-energy (10–15 MeV) γ rays often require separation of γ rays from fast-neutrons and (large) BaF_2 detectors are generally used in such experiments. Bismuth germanate ($Bi_4Ge_3O_{12}$ or BGO) detectors are interesting because of the high-density of the material and the very high-atomic number (83) of bismuth. This makes them extremely efficient, approximately thirty times as efficient as NaI(Tl) detectors per unit volume. In spite of their low light output, they are commonly used today as the Compton suppressors where their high efficiency is very important. Finally, cesium iodide (CsI) scintillators have a higher γ-ray absorption coefficient than NaI(Tl) or BaF_2 scintillators and their decay time component of 630 ns allows for some pulse-shape discrimination (between γ rays and charged particles). An important difference between NaI(Tl) and CsI is that CsI scintillators are not hygroscopic and can be readily used in large arrays of small particle detectors (see, e.g. the microball in section 4.4.2.).

4. Gamma-ray detector arrays

4.1. The first detector arrays

One of the main goals in nuclear structure is to identify new properties of the nucleus. These often emerge in extreme conditions of high angular momentum, high excitation energies, or extreme neutron to proton ratios. However, under these conditions, the states of interest are generally very weakly populated in the reaction: for example a superdeformed (SD) band (a rotational band in a very deformed nucleus) may have an intensity of only 1% of the total γ-ray flux of the nucleus. Therefore, the ability to isolate a given sequence of γ rays from a complex spectrum is an important property of modern γ-ray arrays. Before 1980, nuclear physics experiments were performed with only a few γ-ray detectors. Typically, there were a few Ge(Li) detectors around the target to record high energy-resolution spectra, some NaI detectors to study low energy-resolution spectra, and other detectors to select the starting point of a γ-ray cascade (and therefore reduce the number of cascades to be separated). Examples of the last type are γ-ray multiplicity filters and γ-ray sum-energy spectrometers. The γ-ray multiplicity is the number of γ rays that are emitted in an event. The γ-ray multiplicity filters consisted of a few (of order 6) standard NaI scintillators located close to the reaction point (target) to achieve a relatively high efficiency. Since the number of detectors hit in an event is, on the average, related to the γ-ray multiplicity, high-angular-momentum events that generate many γ rays were selected by requiring a minimum number of hits in the multiplicity filter. Similarly, high-angular-momentum events typically correspond to a large total γ-ray energy which could be selected by using very large NaI scintillators (e.g. two cylindrical detectors approximately 30 cm diameter and 20 cm thick) above and below the target. However, neither of these detectors was selective enough to define a narrow range of multiplicity or total energy in an event, so that the selection of high-angular-momentum events was rather poor.

What the first two arrays, namely the spin spectrometer [24] in the USA and the crystal ball [25, 26] in Germany have done is essentially to sharpen that selection. They consisted of a shell of NaI detectors (72 and 162, respectively) positioned radially around the target and covering close to 4π solid-angle. With the 4π coverage the number of detectors largely determined the selectivity of these arrays: the more detectors, the better the definition of the

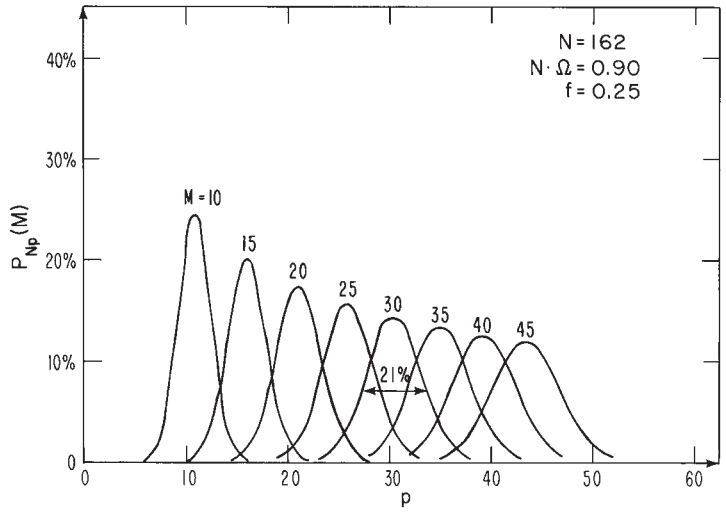

Figure 7. Distributions $P_{Np}(M)$ of the number of hits, p, for various events with M incident γ rays, in a spherical shell of 162 NaI counters with 90% efficiency ($N\Omega$) and 25% probability (f) of Compton scattering.

γ-ray multiplicity. However, each detector was thick enough ($\sim$15 cm) to absorb the γ rays efficiently and had a large enough diameter ($\sim$7 cm) to minimize Compton scattering. Figure 7 shows the distribution of the number of hits in the detectors for various numbers of incident γ rays (or multiplicity M) for a system like the Crystal Ball. One sees that requiring a number of hits p selects a fairly narrow range of multiplicities.

One important limitation of these two arrays was that individual γ-ray energies cannot be obtained on an event-by-event basis except for the few detectors in which a γ ray is detected with no hit in the surrounding detectors (of order 5 γ rays in a high-multiplicity ($M \sim 20$) event). However, the main problem with these NaI detector arrays was that the energy-resolution was poor ($\geqslant$5% at 1.332 MeV). A big advance came with the HPGe arrays which allowed a much higher energy-resolution for the detected γ rays. This increase in sensitivity has been quantified in the concept of resolving power.

4.2. Resolving power of γ-ray detector arrays

The ability of an array to resolve many weakly populated sequences embedded in large and complex backgrounds depends on the detailed nature of both the sequence and the background, so that there is no unique definition of the resolving power. Our definition of the resolving power [27, 28] of such arrays is related to a certain type of spectra. These are γ-ray spectra typically produced in nuclear fusion-evaporation reactions, and consist of a number ($M \sim 20$) of γ rays per cascade separated on the average by an energy, SE. We further assume that the background is essentially uncorrelated with the peaks (which means that the cascade of interest has a small intensity and is not in coincidence with the bulk of the background). To be 'resolved', a peak must stand out above the background and also be statistically significant. We take as a criteria for a peak to be resolved from the background that the peak-to-background ratio is unity and that there must be N counts in the peak. The increase in sensitivity of the arrays comes from the ability to increase this ratio by setting several gates in a multi-dimensional matrix and still retain enough counts in the peak.

The expression [28] of the resolving power RP is:

$$\mathrm{RP} = \exp\left[\frac{\ln(N_0/N)}{(1 - \ln\epsilon_a/\ln R)}\right] \tag{3}$$

where N_0 is the total number of events in the experiment; ϵ_a is the total full-energy peak efficiency for a typical γ-ray energy of 1 MeV; $R = 0.76(SE/\delta E)P/T$ is the increase in peak-to-background ratio obtained for each gate set in a multi-dimensional matrix. We take SE = 60 keV for all resolving power estimates. This formula shows that the important parameters which determine the performance of this type of γ-ray array are the energy-resolution δE of the detectors, their characteristic peak-to-total ratio P/T, and the full-energy peak efficiency ϵ_a. If we take $N = 100$ and a typical value of $N_0 = 2.88 \times 10^{10}$, corresponding to a reaction rate of 10^5 s^{-1} for a duration of 80 h, then $\ln(N_0/N) = 19.5$. Note that this formula requires that R be greater than 1, and therefore it does not apply to arrays with low energy-resolution detectors like the NaI arrays. An important property of the resolving power as defined here is that it is the inverse of the intensity of the weakest cascade that can be resolved in a reaction. For example, a resolving power of 10 000 means that one can resolve a cascade that is 10^{-4} of the total intensity.

4.3. The first-generation high energy-resolution arrays

To understand the structure of the nucleus with some precision, one must reach a high sensitivity, i.e. a high full-energy-peak efficiency as well as a high energy-resolution, so that as many states as possible can be resolved. This is what the high energy-resolution arrays were designed to do. Impressive developments were achieved over the last 20 years and will be reviewed in the remainder of this section.

4.3.1. TESSA0. The first 'high energy-resolution array', called the escape suppressed spectrometer array (TESSA0) was built in 1980 in Risø, Denmark as a joint Niels Bohr Institute (Denmark)/Liverpool University (UK) project. The array [29–31] consisted of 5 Ge(Li) detectors, of relative efficiency ∼25% each surrounded by a NaI Compton suppressor (see figure 8). Each NaI suppressor (shield) was a 25 cm diameter, 20 cm long cylinder positioned around the target as shown in the figure. There were several generic features. (1) The main feature of this array was that the Ge(Li) detectors were Compton-suppressed. The peak-to-total ratio increased from ∼ 20% for the bare Ge(Li) detector to ∼60% with Compton-suppression. (2) Most of the Ge(Li) detectors were located at angles which minimize the Doppler effects, i.e. four detectors were placed at θ of $\pm 52.5^\circ$ and $\pm 142.5^\circ$ to the beam velocity direction. In many experiments, the nucleus under study is recoiling in the target chamber roughly in the incident beam direction at a velocity, v, of a few percent of the speed of light, c. Therefore, the γ rays would be Doppler-shifted according to the following formula:

$$E_\gamma^s = E_\gamma \frac{\sqrt{1 - (v/c)^2}}{1 - (v/c)\cos\theta} \simeq E_\gamma \left(1 + \left(\frac{v}{c}\right)\cos\theta\right), \qquad \left(\frac{v}{c}\right) \ll 1 \tag{4}$$

Since these angles were known, the measured E_γ^s could be corrected to deduce E_γ. However, the Ge(Li) detectors had a finite size and, even at a distance of 25 cm from the target, subtended a non-negligible angle $\Delta\theta$ (in this case $\Delta\theta = 11^\circ$). This meant that within a detector, E_γ^s could vary by $\Delta E_\gamma^s = E_\gamma(v/c)\sin\theta\Delta\theta$ for a given incident γ-ray energy, resulting in a broadening of the γ-ray full-energy peak. This is called the Doppler broadening. For a 1 MeV recorded in a detector located at 90° to the beam and a v/c of ∼3%, ΔE_γ^s is maximum and equal to 6 keV compared with a typical energy-resolution of 2 keV in the

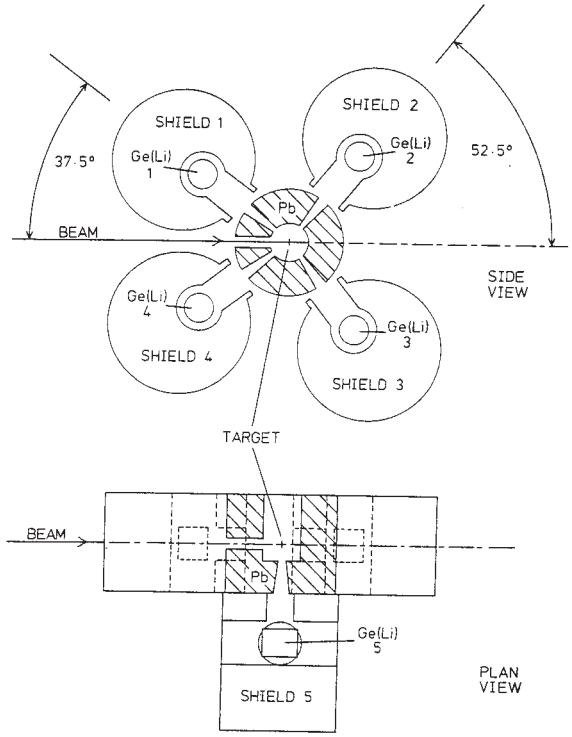

Figure 8. Top: schematic side view (vertical cross section) of the TESSA0 array of five Compton-suppressed Ge(Li) detectors. Bottom: plan view (projection on the horizontal plane). The hatched area represents the lead collimators.

absence of Doppler effects. This Doppler broadening cannot be corrected and this is why four out of five Ge(Li) detectors were located at angles as close as possible to the beam axis (small values of $\sin\theta$). (3) Generally, some detectors have to be located at 90° to the beam because the γ-ray angular distribution gives information on the multipolarity of the γ rays, hence on the spins of the nuclear levels. (4) Collimators were placed in front of the Ge(Li) detectors to restrict the direction from which the γ rays can enter the detector, thus reducing the number of γ rays that scatter from surrounding material into the detector. This further improved the peak-to-total ratio. The collimators also shielded the NaI suppressor from the direct view of the target which would cause false vetos. (5) There was anti-Compton NaI material extending in front of the Ge(Li). This lip suppressed the γ rays that were backscattered out of the Ge(Li) detector and would otherwise have left in the spectrum a peak at $\sim E_\gamma - 0.2$ MeV for incident $E_\gamma \geqslant 1$ MeV (see equation (1)). The size of the NaI suppressors limited the number of Ge(Li) detectors to five. The next arrays that were developed removed this limitation.

4.3.2. HERA. The high energy-resolution array (HERA), was proposed in 1981 [32, 33] at the Lawrence Berkeley National Laboratory (LBNL), USA and built over the next few years. This array pioneered the use of Compton suppressors made of BGO. The array included 21 Compton-suppressed 25% high-purity Ge (CSG) n-type co-axial detectors ($\sim 5 \times 5$) arranged in three rings of 7 around the target as shown in the perspective view of figure 9. The 21 detectors could be used since the volume of each BGO Compton suppressor was

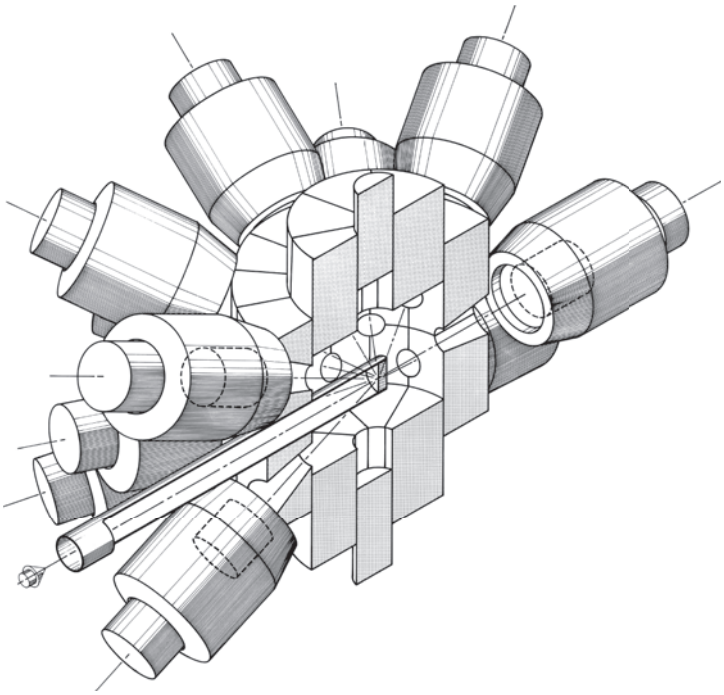

Figure 9. Schematic perspective view of HERA. Only one half of the array is shown surrounding the beam line. The shaded tapered cylinders are the BGO shields, each surrounding a co-axial HPGe detectors (outlined as a dashed cylinder in three BGO shields). The vertical cylindrical sectors are the elements of the BGO central ball.

approximately eight times smaller than that of a NaI suppressor for a similar suppression factor. The BGO suppressors were cylinders 12.5 cm long by 13 cm diameter, beveled at a 20° angle in front so that they could fit closer, with a central axial hole 6.5 cm in diameter. Later, a NaI lip was attached in front of each BGO detector to suppress the backscattered γ rays. The detectors were mostly placed at forward and backward angles to optimize the detection of electric quadrupole γ rays and to minimize the Doppler broadening. In HERA, a BGO 'central ball' of 44 elements, arranged in three concentric cylinders (see figure 9) was placed around the target to record γ-ray multiplicity and total energy in the same way as the crystal ball and the spin spectrometer mentioned above. There were holes in the central ball at appropriate places so that the Ge detectors viewed directly the target but the BGO suppressors did not. Thus the central ball acted as an active collimator.

The peak-to-total ratio in the Compton-suppressed Ge detectors was 0.5 (with a 0.3 MeV threshold) for the 1.332 MeV ^{60}Co line. This large peak-to-total ratio together with the large number of detectors meant that for the first time it was possible to record coincidences with fold >2. The rates gave enough statistics in a standard 80-h experiment to analyse 3-γ correlations. This was a new kind of analysis which allowed one to separate cascades containing three particular γ rays from the larger number of those which contain only two particular γ rays, thereby making use of the higher resolving power of the instrument. In addition, with a peak-to-total ratio of 0.5 (instead of 0.2 for unsuppressed Ge), the full-energy peak correlations represented 25% of the data (instead of 4%) in γ–γ coincidences and 13% (instead of 0.8%) for γ–γ–γ coincidences—an enormous improvement. From equation (3) we find a resolving

power of 50, which means that we can isolate, or 'resolve', a cascade of 2% intensity in the reaction.

4.3.3. Other first-generation arrays. With the advent of BGO suppressors, an explosion of activity led to the construction of many arrays around the world having photopeak efficiencies $N\epsilon_a$ around 0.5–1%. Following TESSA0, a series of TESSA arrays were developed between 1983 and 1988 using BGO Compton suppressors, starting with the TESSA3 array of 12 CSG detectors, up to ESSA30 which comprised 30 CSG detectors [30,31]. Arrays of up to 12 CSG detectors using some asymmetric BGO Compton suppressors were built, for example the OSIRIS array in Germany [34]. In the USA, a 12 CSG array was built at Argonne National Laboratory (ANL) and a 20 CSG array was built at Oak Ridge National Laboratory (ORNL). The two most recent arrays of this generation were also the most sophisticated. The Canadian 8π Spectrometer [35] had a more spherical geometry and consisted of 20 CSG detectors 'looking through' a spherical BGO central ball of 72 elements (of geometry similar to that of the spin spectrometer), resulting in the best multiplicity resolution at that time. However, it had a lower total photopeak efficiency (0.9%) than HERA (1.5%) because the Ge detectors were farther from the target (27 cm instead of 15 cm). A Scandinavian collaboration built the NORDBALL [36] which also consisted of 20 CSG detectors and had several innovations: (1) the Ge detectors were composed of two parts: a front part which is a 1 cm thick crystal and suppresses the γ rays backscattered from the back part which is a co-axial detector, while having little effect on the transmission into the back part for γ rays with energies greater than 400 keV. In turn, detecting a γ ray in the front part, while requiring no signal in the back part, improves the response function for low-energy γ rays; (2) a central ball consisting of a spherical 'shell' of 60 identical BaF_2 elements with holes for viewing the target by the Ge detectors. Because the time resolution of the BaF_2 elements is lower than 300 ps, neutrons can be rejected due to their time-of-flight (which is longer than that of γ rays), providing cleaner sum-energy and γ-ray multiplicity measurements. Finally, there is the 'Chateau de cristal' [37] built by a French collaboration. It uses BaF_2 for 12 composite Compton suppressors as well as for the central ball which comprises 38 elements. Alternatively, the total of 72 BaF_2 elements can be used as a 'crystal ball' similar to the early NaI balls. The BaF_2 material has absorption and resolution properties intermediate between those of NaI and BGO, but it is the timing properties that made this array particularly useful in experiments requiring good timing.

4.3.4. Impact of the first-generation arrays. Because of their relatively high resolving power, these arrays revealed properties of weakly populated nuclear levels (typically down to $\sim$1% of the reaction yield). This often meant levels of high-angular-momentum or of exotic nuclei far from stability. The most spectacular example was the observation of a rotational band in a so-called 'SD' nucleus, ^{152}Dy [38], using TESSA3. SD nuclei can be loosely defined as possessing prolate axially deformed shapes with major-to-minor axis ratios approaching 2 : 1 (compared with $\sim$1.3 : 1 for normally deformed (ND) nuclei). They are the best nuclear rotors known, giving de-excitation spectra (down the rotational bands) consisting of nearly equally spaced γ rays starting from very high spin levels, ($\sim 60\hbar$ in ^{152}Dy). Although these γ rays were buried in a huge background, the key to finding them was to make use of the regularity of the spectra and of the increased efficiency of the multidetector arrays with higher resolving power.

4.4. The second-generation high energy-resolution arrays

The next generation of high energy-resolution arrays represented the state-of-the-art optimization of a Compton-suppressed Ge array, using all the available space (4π solid-angle),

and the biggest Ge detectors available. A little later new concepts emerged which led to an increase in the granularity of the Ge detectors while maintaining, or even increasing, the Ge solid-angle: these are the ideas of composite and segmented detectors. The resolving power of the second-generation arrays is 100 times higher than that of the first-generation arrays. We will review them in this section.

4.4.1. The early second-generation arrays. The first step toward second-generation arrays was to incorporate the largest Ge detectors available and to move toward 4π coverage with these detectors. The first of these arrays to operate were the GASP array [39] at the LNL laboratory in Legnaro, Italy and the Eurogam I array [40] at the Daresbury Laboratory in England, both in 1992. The new feature of these arrays was the use of the large ($\sim 7 \times 8$) $\sim$70% Ge detectors with compact BGO shields. With 40–45 detectors, the resolving power was close to 450.

4.4.2. Gammasphere. Gammasphere [1] represents the optimum design for the second-generation arrays. It was first proposed in 1987 and built as a USA National Facility at LBNL with the participation of Universities and National Laboratories. In contrast with the relatively large number of first-generation arrays which were used by rather small groups, Gammasphere was the single large array built in the USA at the cost of \$20 M. A new feature is that Gammasphere is a movable array, and has been operating at two National Laboratories (ANL and LBNL), making use of the specific opportunities available at each site.

Gammasphere is a '4π' shell of BGO-Compton-suppressed HPGe n-type detectors. The Ge detectors cover 46% of the 4π solid-angle distributed over 110 detectors. Each cylindrical Ge detector is surrounded by a tapered hexagonal BGO shield. The geometrical design of Gammasphere aimed to maximize the detector area while retaining granularity and keeping all detectors very similar in size and shape. In addition, symmetry in the orientation of the detectors was maximized for angular distribution measurements. This design represents the optimum way of tiling a sphere with polygons under the constraints just mentioned [1,25,41], and at a reasonable cost. The result is a configuration of 122 polygons having the symmetry of an icosahedron, with 110 very similar (but irregular) hexagons covering 95% of 4π, and 12 pentagons, as shown in figure 10. The pentagons are not used for CSG detectors, but could be used for other kinds of detectors (e.g. planar Ge detectors for low-energy γ-ray detection) as well as for beam input and exit, anchoring for the support structure, and for the target system.

One Gammasphere module, a HPGe–BGO-suppressor assembly, is shown in figure 11. The Ge detector is as large as could be manufactured at the time, with the front 2 cm tapered with an angle of 7.45° to optimize the BGO thickness in that region. A new feature is the off-centre Ge cooling rod so that a BGO 'back plug' could be placed over most of the back of the Ge detector to suppress the forward-scattered γ rays that escape the Ge material. Each BGO element is a tapered hexagon consisting of six optically separated sectors, 18 cm long, with a lip that extends 3 cm in front of the Ge detector. The distance between the target and the front of the Ge crystal is 25.25 cm. When put together, the array has a BGO honeycomb-like structure with the circular holes filled by the Ge detectors. This makes the thickness of BGO material rather small (0.56 cm) at the thinnest point of each BGO (see figure 11). However, this thickness could be doubled if two adjacent Ge detectors 'share' the BGO material between them: this is called the electronic honeycomb design. In this design, each sector has its own output; however, two adjacent BGO sectors can be combined in software to suppress each of the two adjacent Ge detectors, except when the neighbouring Ge detector is triggered, in which case only the sector closer to the Ge is used. This design minimizes false vetoes which can occur

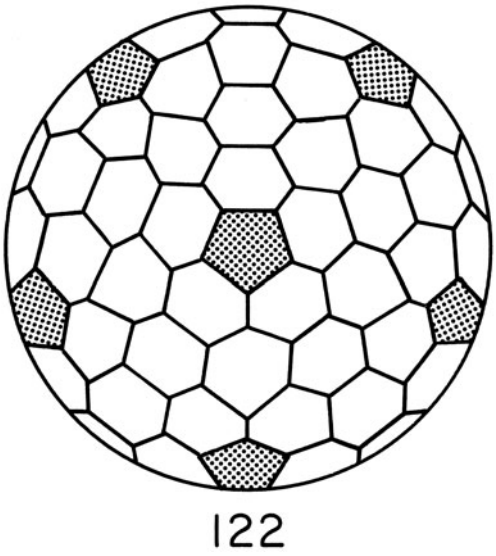

Figure 10. Detector configuration in Gammasphere. It results from the tiling of a sphere with 110 hexagons and 12 pentagons (grey).

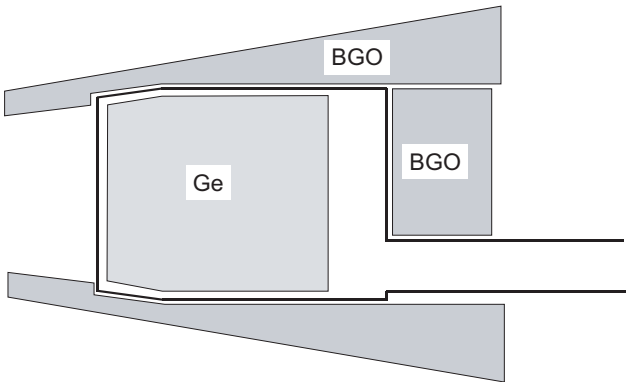

Figure 11. Side view of a Gammasphere module.

when two neighbouring Ge crystals share a single BGO, but provides essentially the same performance as having twice the thickness of BGO. The BGO back plug provides a significant 10% improvement [42, 43] in the P/T ratio which becomes $\sim$0.68.

In Gammasphere, the count rates are very high in a typical fusion–evaporation reaction and events are usually recorded only when at least 5 'clean' (no count in the BGO suppressor) Ge detectors are triggered (5-fold data). For high-multiplicity reactions (average γ-ray multiplicity of 20–30) this still gives a count rate of $\sim$5000 events s^{-1}. Gammasphere became fully operational in early 1996 although it started operating in an Early Implementation stage with 32 modules in March 1993.

Ge detectors segmentation. During Gammasphere construction, it was found that the granularity of the array could be increased without having to redesign the array by electrically segmenting [44] the outer electrode of the Ge detectors, using a lithographic technique.

One could then decide which segment received the incident γ ray by measuring the proportion of energy deposited in each half. This results in a position resolution that corresponds approximately to a third of the angle subtended by the detector. The effective energy-resolution δE of the Ge detectors was improved from $\delta E = 5.5$ keV to 3.9 keV (for v/c of 0.02). Seventy of the 110 Ge detectors were segmented, increasing the resolving power from 1000 (without segmentation) to approximately 3000. Segmentation has an enormous potential for increasing granularity as will become evident.

Gammasphere auxiliary detectors. The power of Gammasphere is increased by using auxiliary detectors to characterize events. One class of these detectors further decreases the γ-ray background by allowing the identification of the nuclei produced in the event. Other auxiliary detectors improve the γ-ray energy-resolution by measuring the velocity of the emitting nucleus on an event-by-event basis, thereby greatly reducing the Doppler broadening. Still others are used to perform special measurements, for example magnetic field devices to measure g-factors of nuclear levels, or so-called recoil-distance plungers to measure some nuclear level lifetimes. We will mention here the four most heavily used devices, the microball, the neutron shell, CHICO, and a recoil detector called the fragment mass analyser.

The microball [45] is a 4π multidetector light charged particle and/or fragment detector built at Washington University, USA (see figure 12). It consists of 95 CsI(Tl) scintillators closely packed to cover a large solid-angle ($\sim$97% of 4π). It has good particle identification (based on pulse-shape discrimination), an adequate granularity, good energy-resolution, excellent stability, and a small total mass. This last property is particularly important since the γ rays traverse this detector before reaching the Ge detectors. Both the γ-ray detection efficiency and P/T are reduced by $\sim$10% with microball in place but this array greatly helps in identifying reaction products which emit charged particles.

Recently, a Neutron Shell [46] was also built at Washington University, USA. It was designed especially for use in conjunction with Gammasphere and often with the microball

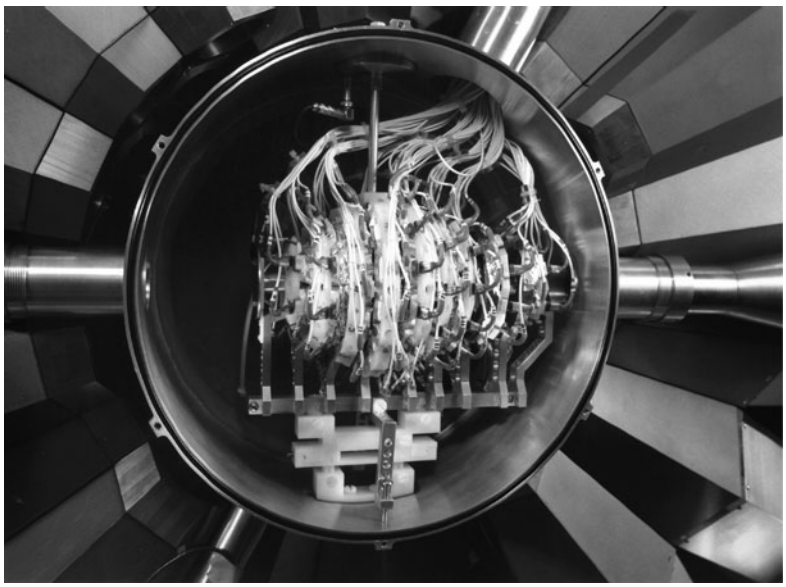

Figure 12. Side view of microball inside the Gammasphere target chamber. The Gammasphere BGO shields with their hevimet collimators are seen surrounding the target chamber.

for selecting very weak one- and two-neutron-evaporation channels in very neutron deficient systems, again considerably increasing the sensitivity of Gammasphere. The array consists of up to 30 tapered regular hexagonal neutron detectors whose sensitive component is the liquid scintillator BC501A coupled to a 5-inch photomultiplier tube. These detectors can replace the 30 most forward Ge-BGO modules of Gammasphere.

The heavy-ion detector CHICO [47] was built at the University of Rochester, USA. It is a powerful array of 20 parallel plate avalanche counters (PPACs) which fits within the Gammasphere target chamber. In some nuclear studies, such as Coulomb excitation, the two interacting nuclei do not fuse but scatter through a broad range of angles. This results in very broad γ-ray lines due to the wide range of Doppler shifts. The CHICO detector determines, with good accuracy, the direction of each emerging nucleus. The PPACs arrangement has the same five-fold symmetry as the Gammasphere Ge detectors (which greatly simplifies the analysis) and the solid-angle coverage is 2.8π. The PPACs are configured into two co-axial cones (with 10 faces each) backward and forward around the beam direction with bases that join in the vertical plane of the target. Each PPAC anode and cathode is segmented such that it provides an angular accuracy of 1° for the polar scattering angle and of 9° in the azimuthal angle. This, together with an excellent time resolution of 500 ps, completely determines the kinematics of each nucleus in the collision.

The fragment mass analyser [48] is a recoil mass separator that has been coupled to Gammasphere at ANL. It allows selection of low-yield fusion recoils through a measurement of the mass/charge ratio and can be augmented by the detection of the characteristic alpha decay of this product in a focal plane double-sided Si Strip detector (the recoil decay tagging technique).

4.4.3. Euroball. Large gains in performance can come from three factors: (i) using 100% of the 4π solid-angle for Ge detectors (eliminating the Compton suppressors); (ii) increasing the granularity sufficiently to recover the intrinsic resolution of the Ge detector (by eliminating the Doppler broadening); and (iii) increasing the absolute intrinsic efficiency ϵ_p by recovering the photons that have Compton-scattered out of a Ge detector. This is the concept behind the tracking arrays. In the early 1990s, steps in this direction were accomplished with the fabrication of composite and segmented detectors. Gammasphere exploited segmentation. Concurrently, another approach emphasizing composite detectors was used in Euroball.

Clover detectors [49] consist (see figure 13) of four detectors (initially $\sim 5 \times 7$) each tapered in front into a square shape 42 mm on a side and closely packed in the same cryostat into a 'four-leaf clover' configuration. Such a detector 'simulates' a very large Ge detector with, in this case, a relative photopeak efficiency of 140%. The photopeak efficiency is 1.5 times the sum of the individual detectors' photopeak efficiency due to the adding back of signals that scatter between crystals. The separation into four detectors reduces the Doppler broadening of a clover detector to approximately two thirds of that of a single detector of the same size as the full clover assembly [50]. The sensitivity to neutron damage is also reduced (again as compared with a single detector of the same size). Such clover detectors are most effectively used at 90° to the beam direction where the Doppler broadening is maximum. They were used for the first time in the Eurogam II [12, 49] array in Strasbourg, France. Each clover detector was surrounded by a BGO Compton suppressor, bringing its P/T ratio to 0.55. The resolving power ($\sim$950) was twice that of Eurogam I.

Cluster detectors [51–54] represented the next step in composite detectors. By grouping seven (60%) Ge detectors in a single cryostat (see figure 14) in add-back mode (see section 1) and surrounding them by a Compton suppressor, an impressive intrinsic photopeak efficiency ϵ_p of 0.3 can be achieved (compared with 0.22 for a Gammasphere detector) with a P/T ratio

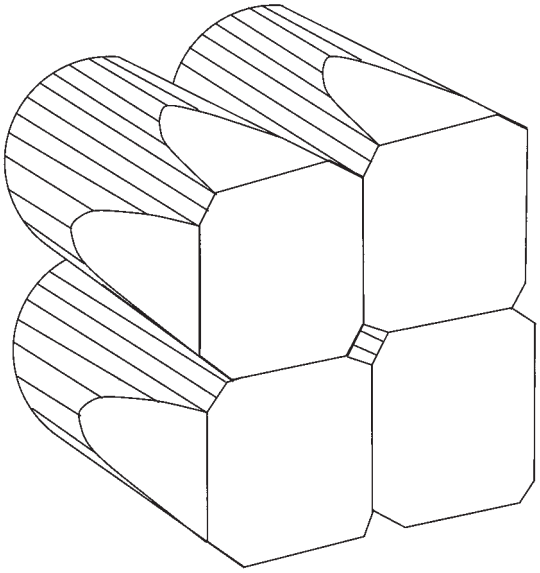

Figure 13. Schematic view of a clover detector.

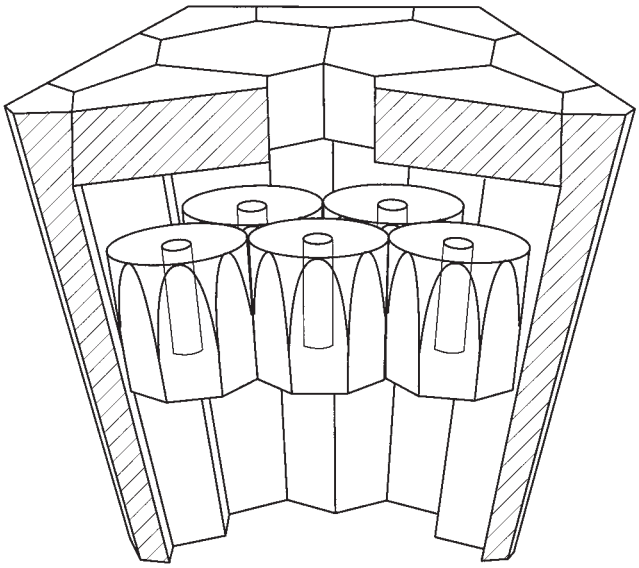

Figure 14. Schematic diagram (side view cross section) of a cluster of 7 HPGe detectors (5 visible) surrounded by their BGO Compton suppressor (hatched cross section).

of 0.63. The BGO shield consisted of 18 optically separated elements, 12 surrounding the sides of the Ge cluster and 6 back plugs behind the Ge detectors. The difficulty of building and operating seven Ge detectors within a single cryostat triggered the development of so-called encapsulated HPGe detectors [51, 53] by a collaboration of the University of Köln, the KFA of Jülich and the company Eurisys Measures. In the current design [51] (figure 15), the Ge detector, hexagonal at the front and circular at the rear, is encased in an aluminium can 0.7 mm

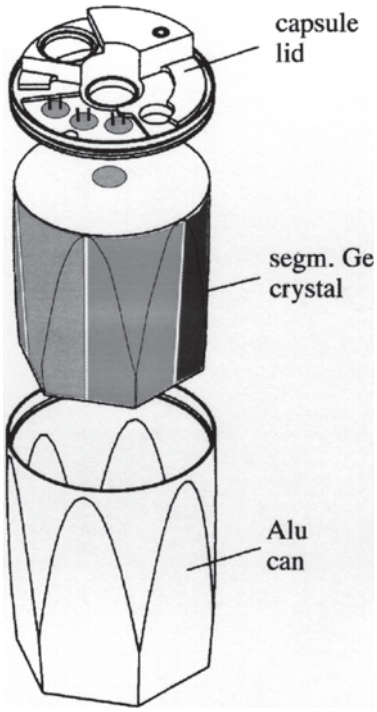

Figure 15. Components of an encapsulated Ge detector.

thick and the internal distance between the Ge surface and the can is 0.5 mm, much smaller than the 5 mm distance in conventional Ge detectors. The capsule is hermetically sealed by electron welding of all feedthroughs and the lid. Thus the detector vacuum is separated from the cryostat vacuum, and the seven 'capsules' are closely packed in a common cryostat. This has several advantages: the crystal remains sealed at all times, which avoids contamination of the Ge surfaces which can happen for example when annealing detectors; annealing is greatly simplified since one just needs to set the capsule in an ordinary oven, the vacuum within the capsule remaining below 10^{-6} mbar; the cold FET is outside the capsule and can be easily repaired and also removed before annealing; a defective Ge detector in a cluster can be replaced with minimal effort. It is worth noting that the cluster detectors have an excellent efficiency for high-energy γ rays [54]: the quality of a 10 MeV γ-ray spectrum is as good as that of a 1 MeV γ ray detected with a conventional (e.g. Gammasphere) Ge detector. Fifteen such clusters were built as part of the Euroball.

Euroball [13] is a 4π array built by a collaboration from France, UK, Germany, Italy, Denmark and Sweden. It combines the three detector types that have been developed in the 1990s and started taking data in Legnaro, Italy, in early 1997. In the forward (beam) direction (see figure 16) 30 of the large CSG detectors used in GASP and Eurogam I are closely packed at a distance of 37.5 cm from the target. Around the 90° direction to the beam a solid-angle of 2π is covered by two rings of 13 clover detectors each, most at 26.5 cm from the target. In the backward direction, the 15 cluster detectors, each with their Compton suppressor, are located at a distance of 44.5 cm from the target. Although more difficult to use than Gammasphere because of the very different types of detectors involved, Euroball has a similar resolving power. Euroball has a suite of auxiliary detectors which further increases its resolving power. The most

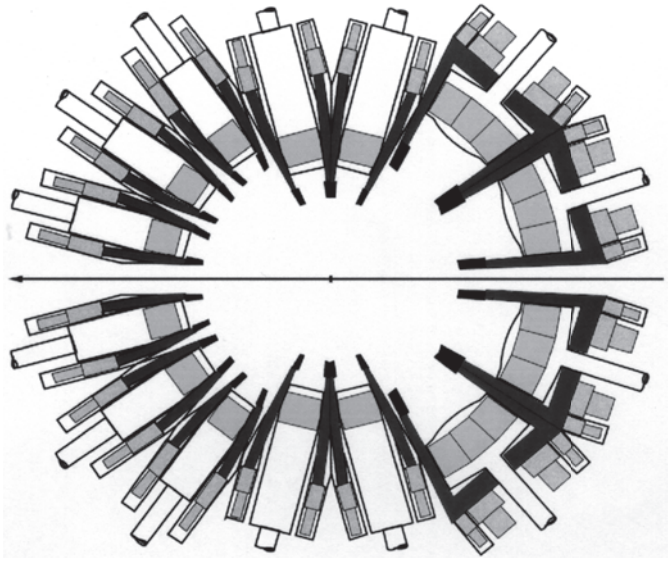

Figure 16. Schematic view (side cross section) of Euroball.

unique of these is a central ball of 210 BGO detectors [55]. The central ball elements, the Ge elements and the BGO Compton-suppressor elements are regrouped into 164 subunits of equal efficiency and solid-angle used to determine the total γ-ray energy and γ-ray multiplicity in an experiment. Euroball has been used at LNL in Legnaro (Italy) and at Institut de Recherches Subatomiques (IReS) in Strasbourg (France).

4.4.4. Impact of the second-generation high-resolution arrays. The 100-fold increase in resolving power of these arrays (as compared to the first-generation arrays) means that one can study features that are 100 times weaker than before. In nuclei, it means, for example, understanding structures at higher angular-momentum, higher temperature or for more exotic nuclei. An example of the increased power of these new arrays is the discovery of the 'linking transitions' between SD states and ND states in some nuclei around mass 190 [56–58] and mass 150 [59]. These transitions are indeed very weak, around 1% of the intensity of the SD bands (which themselves have an intensity around 1% of the total cross section) and their observation corresponds to the gain made possible by the increase in resolving power. Observing these 'SD decay' transitions aids in the understanding of how the nucleus makes such a dramatic transition between two states in which the shapes are very different. The decay spectrum from the SD state is similar to the statistical decay spectrum of a highly excited ND state, suggesting that the decay arises from a small admixture ($\sim$0.5%) of the (high-density) ND states into the SD state. These links have been observed in very few cases (3 out of about 350 bands known) and the full decay mechanism is still not clear. Many failed searches in other nuclei indicate that higher resolving power is needed to elucidate completely the decay mechanism of SD bands.

4.5. Recent developments in increasing granularity

Some arrays now under construction are geared toward a very high full-energy peak efficiency. This is a critical property because these arrays are meant to be used with radioactive beam

accelerators which inherently provide beams of low intensity. In addition, in many of these 'exotic' nuclei studies, the angular momentum of the product nuclei, and therefore the γ-ray multiplicity, is low and this allows the use of larger detectors closer to the target. However, it is necessary to achieve a good energy-resolution if the full-energy peaks are to stand out above the background. This requires a high granularity, in order to reduce the large Doppler broadening associated with the (often) large velocities of the recoiling nuclei. In the arrays being built for this purpose, the design of the detector units uses a combination of composite and segmented detectors.

One array, called EXOGAM [60, 61] (see table 1), is developed by a European collaboration and consists of up to 16 detector units which can be arranged in various configurations depending on the study to be made. Each unit is a 4-crystal segmented clover detector with each of the Ge crystals electrically segmented in the azimuthal direction into four equal segments (4×1). The clover is Compton-suppressed by a modular BGO shield consisting of independent side shields, rear-side shields, and back catchers. The side shields can be removed to obtain a more compact geometry where the sides of the clover detectors touch. For a Coulomb excitation experiment (assuming that the recoil angle has been measured with an accuracy of 3°) with a γ-ray multiplicity of 2 and a recoil-velocity v/c of 7.5% of the speed of light, and for a γ-ray energy of 1.33 MeV, the photopeak efficiency ϵ_a is 0.18 (almost twice that of Gammasphere and Euroball), the P/T ratio is 0.45 and the energy-resolution is 14.9 keV for a target-to-crystal distance of 11.4 cm. In Canada, its counterpart TIGRESS [62] is currently under consideration. It has an additional two-fold longitudinal segmentation (4×2).

Another array, called MINIBALL [54, 63, 64], developed by a European collaboration, is also operational. It consists of eight cryostats with three Ge detectors in each plus four cryostats with four Ge detectors in each. The Ge detectors are encapsulated and electrically segmented into (6×1) segments. The cluster granularity is thus multiplied by a factor six. The detector-target distance is ~11 cm and for a recoil-velocity v/c of 4.5% the energy-resolution is ~7 keV for a 1.3 MeV γ ray emitted at 90° to the beam. The full-energy peak efficiency ϵ_a is expected to be 0.17 and the P/T ratio 0.5. Also in this case various geometries can be accommodated. Both arrays can be used with auxiliary detectors in order to enhance their power.

In the USA, a position-sensitive Ge-detector array called SeGA [65] is in operation at Michigan State University. It consists of 18 highly segmented HPGe cylindrical detectors, with 4×8 segments. The segments in the longitudinal direction are each approximately 10 mm wide. The axis of each detector is perpendicular to the target-detector direction and tangent to the meridian that defines the detector position so that the opening angle for each segment that

Table 1. Arrays of segmented detectors (more than two-fold segmented).

Name	No of crystals	Size[a]	Shape	No of segments[b]	Crystals/ cryostat	Status
EXOGAM[c]	64	6×7	Square	4×1	4	Operational
TIGRESS[d]	64	6×9	Square	4×2	4	Prototype
MINIBALL[e]	40	7×7.8	Reg. hexagon	6×1	3, 4	Operational
SeGA[f]	18	7×8	Cylinder	4×8	1	Operational
GRETA[g]	120	8×9	Irr. hexagons	6×6	3	Prototype
AGATA[h]	180	8×9	Irr. hexagons	6×6	3	Prototype

[a] Diameter × length in cm before shaping. [b] Azimuth × length. [c] GANIL, France [60, 61]. [d] TRIUMF, Canada [62]. [e] REX-ISOLDE, Germany [54, 63, 64]. [f] Michigan State University, USA [65]. [g] USA [28, 78]. [h] Europe [76].

views the recoils (and therefore the Doppler broadening) is small, determined by the 10 mm segments. For a recoil-velocity v/c of 35% and a 1.3 MeV γ ray, the calculated photopeak efficiency is 2.3% and the energy-resolution is 20 keV (at the typical distance of 20 cm from the target). The overriding concern is the determination of the first interaction point of the γ rays in the detector in order to correct for the very large Doppler broadening. Since there are many small segments, an incident γ ray will trigger several of them, and a scheme needs to be developed to determine the segment where the first interaction occurred. At present, the first interaction is assumed to occur in the segment where the highest energy is deposited. We have seen that the arrangement of composite segmented detectors in various arrays considerably improves the photopeak efficiency and the energy-resolution when observing γ rays of low-multiplicity and at reasonably low rates from fast-moving recoils. The challenge of making a high-rate, high-multiplicity, general purpose detector array that fully exploits these new properties leads to the tracking detectors. The concept of tracking [28] will be discussed in section 6.

5. Advances in electronics and data acquisition

In this section, we will briefly review the electronics and data acquisition systems used in modern nuclear physics experiments to record data from large γ-ray detector arrays.

5.1. Basic scheme of electronics and data acquisition system

The function of the electronic signal processing system is to determine the energy, time and position of the γ ray from the detector pulse. In an 'analog' system, as shown in figure 5, separated pulse shaping (filter) circuits optimized for energy and time measurements are used to produce pulses for an analog to digital converter (ADC) and a time to digital converter (TDC). In a 'digital' signal processing system, the entire pulse-shape is digitized, and the filtering and the energy and time determination are carried out using digital processing. The basic design principle of the filters is the same whether they are implemented in an analog circuit or in digital processing algorithms. However, digital processing provides more flexibility and the possibility of more complicated processing.

The data acquisition system collects the digitized information from the individual detectors and forms the 'event'. Various levels of event selection, formatting, and monitoring are performed by the system. Some are realized more efficiently in the electronics hardware, e.g. coincidence requirements and multiplicity selections. Others, such as energy and time calibration and the selection (gating) of energy and time, are usually carried out in computers. The accepted events are stored on mass storage devices, usually magnetic tape or magnetic disks. During the experiment spectra are generated for on-line monitoring. In the following, we will discuss the components of a typical 'analog' signal processing (see figure 5) and data acquisition system, and mention the recent advances. Later, in section 7, we discuss briefly new 'digital' systems being implemented.

5.2. Modern electronic systems

5.2.1. Preamplifier. The first stage of the signal processing system is the preamplifier. It provides sufficient gain and appropriate impedance matching such that the output signal can be transmitted through a reasonable length of cable to the main data processing system. The noise introduced by the subsequent stages will be negligible compared with that of the preamplifier. The input of the preamplifier (the gate of the FET [20]) is usually connected (DC coupling) [19]

directly to the electrode which is at the ground of the bias voltage. However, when signals from both electrodes are needed, e.g. in a segmented detector, the preamplifier for the electrode with the bias voltage (the central electrode) has to be connected through a capacitor (AC coupling) to block the high voltage. The coupling capacitor will introduce additional noise and could degrade the resolution at high counting rates.

To make the output signal independent of the variation of the detector capacitance (which may fluctuate, e.g. due to changes in surface states), the preamplifier is operated in the charge-sensitive mode: the amplitude of the output voltage signal is proportional to Q/C_f where Q is the charge accumulated at the detector electrodes and C_f is the so-called feedback capacitance of the preamplifier which is fixed. To prevent charge build-up of the feedback capacitor, a pulse-reset circuit [19] produces a short (few microsecond) pulse to neutralize the accumulated charge when the preamplifier output reaches a preset level. This method is used in Gammasphere.

5.2.2. Pulse shaping amplifiers for energy determination. The main amplifier takes the signal from the preamplifier and produces an output signal with the shape and amplitude required by the ADC for the energy determination. The most important requirement is to shape the pulse to achieve the best signal-to-noise ratio, which will produce the best energy-resolution. The so-called peak-sensing ADC, which is used most commonly, requires the pulse-height to be proportional to the charge collected by the detector. In addition, high counting rate capability and insensitivity to the rise-time of the pulse are also important in the selection of the pulse-shape.

There are two important timescales in the design of the amplifier. One is the charge collection time of the detector. Since the charge drift velocity is about $10\,\mathrm{cm}\,\mu\mathrm{s}^{-1}$, the charge collection time for a large co-axial Ge detector is of order several hundred nanoseconds. In order to have the pulse-height independent of the variation of the collection time, the pulse should have a flat top duration longer than this time. The other timescale is the optimal pulse width in order to minimize the noise [19]. For a typical large co-axial detector and cold FET the pulse width which minimizes the noise is in the range of 5–20 μs.

A variety of amplifier shaping circuits [66] have been used to achieve this goal. A quasi-trapezoidal shaper was implemented for Gammmasphere using a single differentiator and by mixing the output of four active integrators to approximate the trapezoidal shape [19]. It has a peaking time of 4 μs and a flat top time of 1 μs. This shape provides low noise and good performance at high counting rates. It also eliminates the so-called ballistic deficit which refers to small losses in the amplifier output signal amplitude due to a long charge collection time in the detector. Ballistic deficit occurs because the various time constants used cannot be arbitrarily large. This is important in larger co-axial Ge detectors which have more rise-time variation with the γ-ray interaction position. One can correct this deficit by calculating it for each pulse based on the known rise-time and amplifier characteristics. Finally, when using high count rates, linear pulses out of the amplifier may overlap too often and degrade the energy-resolution. Pile-up rejector circuits simply reject both signals when the time interval between the two pulses is less than their width.

5.2.3. ADC. The ADC converts the pulse-height of the amplifier output to a digital number (channel). The modern ADCs are based on the successive approximation method [67], which can produce a 16-bit number (for a spectrum with $2^{16} = 65\,536$ channels) in several microseconds. This time is comparable to the pulse shaping time, and thus it does not contribute significantly to the dead time of the data acquisition system. The linearity of the ADC is important to the high-resolution needed in γ-ray spectroscopy. In particular, the differential

non-linearity (DNL), the variation of the width of a channel, is large (about 50%). This will produce a large variation in a spectrum having a flat distribution of pulse amplitudes. This variation can be reduced [68] by averaging channel widths over many channels. This is accomplished by adding a random pulse-height and then subtracting the digital equivalent. This method reduces the DNL to an acceptable level. For example, the Gammasphere high-resolution energy signal uses a 16-bit ADC (with a 4 μs conversion time) and a DNL of 1% is achieved. Also, spectra constructed from a large number of detectors (ADCs), will have a further reduction of DNL, proportional to the square root of the number of detectors.

5.2.4. Time. The timing circuit takes the signal from the preamplifier, shapes it, and sends it to a timing discriminator, which provides a fast timing signal. The time difference of this signal and a reference time signal is digitized by a TDC and recorded. The pulse-shape required for timing is different from that for energy. The shaping circuit reduces the noise and maintains the fast rise-time of the signal. Thus, the timescale of the shaping circuit should be in the range of the charge collection time of the detector, which for a large Ge detector is 300–500 ns. The most commonly used circuit is a constant fraction discriminator (see section 3.2.3). For a large co-axial detector, the time resolution is typically in the range of 5–10 ns due to the rather long charge collection time and the variation of the pulse-shapes in the more complex electric field configuration (especially at the closed-end of the detector).

5.2.5. Trigger and read out. The trigger system uses the characteristics of an event to decide whether to accept the event or not. In a large array, triggering is generally carried out at several levels. The first level is usually implemented in electronics hardware using logic circuits. In a Compton shielded Ge detector array, logical signals produced by the discriminators on the Ge and BGO signals are used to perform the Compton rejection, and to determine the coincidence folds (see section 2.4) of the 'clean' Ge (no signal detected in its shield) and 'dirty' Ge (signal detected in shield) detectors using multiplicity logic circuits. An approximate selection of the angular-momentum of the event can be achieved quickly by selecting these 'fold' numbers. More complex triggers based on the energy and time of γ rays, the total energy of the event, and the γ-ray angular distribution are generated in the next level of trigger, usually implemented in computer software.

The readout system works closely with the trigger system, especially in a data acquisition system with multi-level triggers. After a successful first-level trigger, the readout system reads out all the data from the detectors which have produced a signal, and combines them in a predetermined format. Once the event has been 'formed', it can be sent to different data paths (including data storage, analysis for on-line monitoring, and/or further triggering) before it is stored.

5.2.6. Data acquisition rate. As new generations of arrays became available, the data rate has become a more important consideration in a data acquisition system. As discussed earlier, the requirement to reduce the noise for energy measurement means that the energy signal has to be integrated for a time period of about 10 μs. This determines the time during which a second pulse will pile-up with the first pulse, and appreciable pulse pile-up will occur at a detector counting rate above 10 000 Hz. When two pulses pile-up, the amplitude of both pulses will be destroyed, and the combined signal will produce a background event. A pile-up rejection circuit which examines the time separation between two consecutive pulses is used to reject these pulses.

The time for the ADC and TDC to convert the analog signals to digital numbers is a few microseconds using currently available circuits. This time is comparable to the fall time of the energy pulses, and thus it does not add much to the dead time of the individual detector channel. Overall, the readout would take about 10 μs per event, leading to a total dead time of 20 μs. For a system with pipelining, the ADCs can be active during the readout time and the dead time is thus reduced. In a typical Gammasphere experiment, about 1 Mb s^{-1} of data is stored on 8 mm magnetic tapes.

5.2.7. Implementation of electronics for large arrays. Most of the electronics discussed above are available commercially. They are implemented as NIM, CAMAC and VME modules, and require interconnection between them. If we use these modules for a large array with about 100 elements, the number of modules could reach several hundred and the number of connections could reach several thousand. That would present problems in space requirement, power requirement, and reliability. Instead, all second-generation arrays are using custom-built electronics with a higher level of integration. This is achieved by placing all electronics for one detector module (Ge and BGO shield) on one circuit board, and placing multiple circuit boards in one electronics module, or by grouping circuit boards for several Ge (or BGO) detectors in one electronic module. There are several technologies for constructing circuit boards to achieve high component density: surface mount devices (SMD), hybrid circuits and application specific integrated circuits (ASIC). For example, Gammasphere with 110 channels chose the SMD, while Euroball with 239 Ge channels uses the more compact ASIC technology [12, 69, 70]. The design of high-density electronics has to take into account possible cross talk between channels, heat dissipation and ease of repair.

6. Towards the future: gamma-ray tracking arrays

In a pure Ge array, the removal of the Compton suppressors would increase the Ge solid-angle coverage by roughly a factor of two, and in addition, would recover the full-energy of a γ ray that escapes from one detector to another, increasing the efficiency for the detection of a 1.3 MeV γ ray by another factor of two. Thus, the efficiency for detecting the full-energy of a 1.3 MeV γ ray for a 4π shell of Ge detectors can be estimated to be about 60%, limited only by the finite thickness of the Ge crystals, the gaps and the absorption in the support structures. However, the inability to distinguish between two γ rays detected simultaneously in two detectors and one γ ray interacting in the two detectors has prevented the introduction of pure Ge shells for nuclear physics experiments. To isolate multiple (e.g. 20) simultaneous γ rays sufficiently, more than 1000 detectors would be required whose cost would be prohibitive.

The solution (see figure 17) is to track the interactions of all γ rays in order to identify and separate the emitted γ rays even if several interact in one detector. Taking advantage of the technological advances in segmenting Ge crystals electrically in two dimensions, it is now feasible to build an array of approximately 100 highly segmented Ge detectors. Such an array retains high efficiency by allowing the pulse-shape analysis of signals from each segment to be used to reconstruct the energy and three-dimensional positions of all γ-ray interactions and then track the γ rays. The ability to track the interactions of γ rays in the detector could increase the sensitivity for detecting γ radiation dramatically and might be a step comparable with the first introduction of Ge detectors about 40 years ago.

In the following, we will introduce the tracking concept. We will then briefly mention the various planned tracking arrays before presenting one of them (GRETA) in more detail.

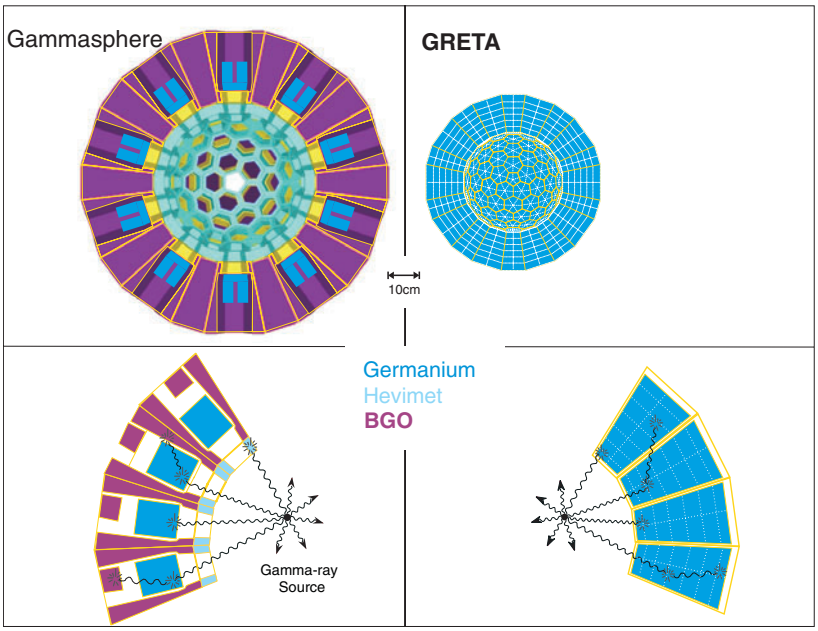

Figure 17. Comparison between the current state-of-the-art detector Gammasphere (left) and the proposed GRETA array (right). In the top part, both instruments are shown on the same scale. The lower portion (not to scale) indicates the two different approaches. While anti-Compton shields suppress cross scattering between Ge crystals and hevimet absorbers prevent direct hits of the shields and thereby false suppression, a γ ray tracking array accepts all γ rays, thereby significantly increasing the efficiency.

6.1. Tracking principle

Tracking of γ radiation [71] requires the determination of individual γ-ray interactions and their scattering sequence, i.e. the time order. Due to the small distance between interactions (a few centimetres to a few millimetres) and a time resolution of typically 5 ns in Ge detectors, it is not possible to determine the time sequence by measuring the time of the interactions. We have to use tracking algorithms, which rely on the characteristics of the underlying physical processes (Compton scattering, pair production and photoelectric effect) to order the individual interactions into a γ-ray path.

6.1.1. Compton scattering. For most γ-spectroscopy experiments (e.g. for γ-ray energies between 150 keV and 8 MeV) Compton scattering is the dominant interaction process. For example, a 1.3 MeV γ ray undergoes on average three Compton scattering processes before it is fully absorbed by a photoelectric effect. Figure 18 illustrates a scattering scenario of an incident γ ray undergoing two Compton scatterings and then a photoelectric absorption. The γ-ray scattering angle is θ, E_γ is the initial γ-ray energy and E_i ($i = 1, 3$) is the energy deposited at the interaction point. Since the range of electrons for γ-ray energies of interest is mostly below 1 mm, the energy deposition is assumed to be at the position of the scattering for the following discussions. Assuming the full-energy E_γ is deposited in the detector ($E_\gamma = E_1 + E_2 + E_3$), and the γ ray is emitted from the source position, it is possible to calculate the scattering angle θ_c for each interaction according to equation (1). In addition, the measured scattering angle θ_m can be deduced from the three-dimensional positions of the interactions. One can define a

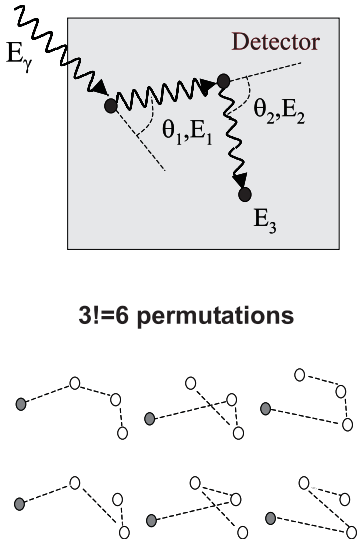

Figure 18. Example of a typical scattering process for a 1 MeV γ ray interacting with a Ge detector. An incident γ ray with the energy E_γ interacts two times by means of Compton scattering before it is fully absorbed by means of the photoelectric effect. The lower part shows all possible scattering sequences which have to be sampled during the γ-ray tracking procedure. The black dot represents the source.

figure-of-merit such as,

$$\chi_j^2 = \sum_{n=1}^{N-1} \left(\frac{\theta_m - \theta_c}{\sigma_\theta} \right)_n^2 \tag{5}$$

where σ_θ is the estimated angle uncertainty and the index j indicates one of the possible sequences (all of which are sketched in figure 18 as well as the source shown as a solid point). It is possible to find the sequence with minimum χ^2. If the interaction points had perfect position and energy-resolution, the tracking would be exact and the properly identified scattering path would show no deviation from the scattering formula ($\chi^2 = 0$). Any deviation would indicate a Compton escape event in which a γ ray left only a fraction of its energy before it scattered out of the detector, or in which the γ ray does not originate from the source. In this way, the γ-ray tracking procedure would work as an anti-Compton detector without the shield. In the ideal case of perfect position and energy-resolution, the peak-to-total ratio would be unity since all escape events would be identified and disregarded and only full-energy events would be accepted.

Unfortunately, due to the finite energy and position resolution in the γ-ray detection system, χ^2 will always be larger than zero and the peak-to-total ratio will always be smaller than unity. Figure 19 shows calculated χ^2 values for full-energy and escape (background) events. Here, γ rays with an energy of 1 MeV were simulated in an ideal Ge shell. Depending on the χ^2 value which is used to separate full-energy (peak) from escape (background) events, it is possible to improve the P/T ratio at the cost of efficiency or vice versa.

6.1.2. Position resolution requirement for tracking. The realization of an efficient tracking array requires a position resolution of 1–2 mm [71] and an energy-resolution of a 2–3 keV per interaction. The required position resolution corresponds to an effective granularity of approximately 30 000 voxels per Ge detector with a volume of 300 cm^3, which is impossible

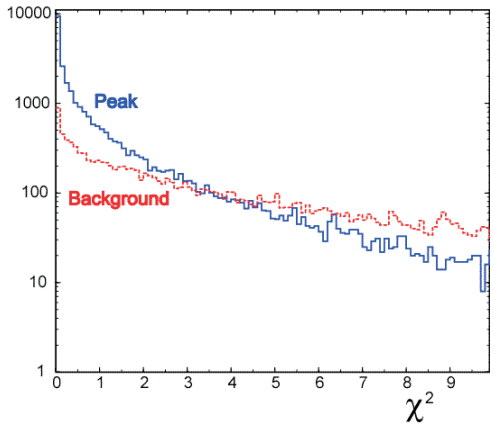

Figure 19. Distribution of χ^2 values for 1 MeV γ rays in a standard Ge shell.

to achieve by a physical segmentation of the crystal. However, pulse-shape analysis methods [72, 73] have been developed, which can provide this position accuracy together with high-resolution energy information. These methods require a segmentation of the outer detector contact into 20–40 segments.

6.2. Planned detector systems

The idea of three-dimensional γ-ray tracking in a solid state detector was conceived at LBNL in 1994. The implementation of these new concepts was called GRETA. European efforts to realize a γ-ray tracking array were first initiated in Italy shortly after with a system called mini array of segmented detectors (MARS). Broader support in Europe was reflected in the establishment of a European wide network, called Training and Mobility of Researchers (TMR) [74], to coordinate the wide variety of efforts. In 2000, these efforts culminated in establishing the advanced gamma-ray tracking array (AGATA) project which is currently the European focus. Table 1 also gives a summary of the characteristics of AGATA and GRETA.

In the following subsections, we discuss briefly these recent efforts to build 4π arrangements of segmented and large volume co-axial detectors and we also discuss possible planar arrays. GRETA will be reviewed in more detail in section 7.

6.2.1. MARS. MARS [75], aimed at building a smaller scale array consisting of 50–60 co-axial HPGe detectors with a two-dimensional 4×6 segmentation in a barrel-like arrangement. A geodesic geometry would be less efficient because of relatively bigger gaps and the loss of material due to the large taper required. The barrel-like structure is more efficient but requires long crystals in order to cover better the equatorial area around 90°. However, count rates are then distributed unevenly among detectors and segments, and significant cross-scattering occurs throughout the whole array. Research and Development for MARS has now been incorporated into the bigger project AGATA.

6.2.2. AGATA. A number of European efforts were initiated after MARS, all culminating recently in the AGATA project [76]. The original design consists of 180 hexagonal and 12 pentagonal Ge detectors in a geodesic configuration. The larger number of detectors permits a larger inner space (34 cm diameter) to accommodate auxiliary devices. Using pulse-shape

analysis tools and tracking algorithms which have been developed in Europe one expects an efficiency of 25% for a cascade of 30 γ rays of 1 MeV and v/c <0.5.

6.2.3. Planar arrays. A possibility for achieving the required position resolution of a few millimetres without pulse-shape analysis is to use detector systems having sufficient pixalation. Such systems might be built [77] of stacks of thin planar detectors, each with one electrode highly pixilated or in double-sided strip (DSSD) configuration where the opposite electrodes are divided in orthogonal strips. To ensure that a single-interaction occurs in one pixel, small pixels or strips are used as well as thin detector layers. The interaction position is determined by the pixel and layer number. In a thicker detector, the measured drift time can determine the interaction depth. Only the energy has to be processed, which can be accomplished by conventional analog processing electronics with very many channels. However, dead layers, e.g. in guard rings, at the edge of each planar crystal, as well as the mechanical structure required to provide sufficient cooling to the HPGe detectors, significantly limit the possibility of assembling these detectors into efficient 4π arrays. Thus, closed-end co-axial detectors are the only feasible choice for constructing 4π arrays at the present time.

7. GRETA

In this section, we will discuss in more detail the design of GRETA, its expected performance, the project status and the new physics opportunities.

7.1. The GRETA design

As indicated in figure 17, the GRETA design consists of a spherical shell, in a geodesic configuration, of 120–130 highly segmented HPGe detectors. To maximize the solid-angle coverage, the detectors are tapered hexagons and pentagons. An isotropic spherical geometry provides nearly equal count rates per solid-angle, which simplifies processing requirements as well data analysis and minimizes scattering processes within the array. However, the space between detectors limits the solid-angle coverage and therefore has to be minimized.

While most of the technology to build Gammasphere was available when Gammasphere was conceived, the segmentation technology, the pulse-shape analysis, and the tracking algorithms were not sufficiently developed prior to GRETA in order to ensure the feasibility of a γ-ray tracking array. Therefore, we will discuss these three aspects in more detail.

7.1.1. Segmentation. The 36-fold segmented GRETA prototype [72] and its segmentation scheme are shown in figure 20. The prototype consists of a closed-ended HP-Ge n-type crystal with a tapered hexagonal shape. The bias is applied to the central contact, which allows the segments to be DC-coupled to the preamplifier (see section 5). The inner hole has a length of 7.5 cm and a diameter of 1.0 cm. The angle of the taper is 10°. The outer electrode is divided into 36 parts (6 × 6). The 6 longitudinal boundaries are located in the middle of the flat surfaces of the hexagonal shape. The widths of the segments along the symmetry axis, starting at the front (the narrow end), are 7.5 mm, 7.5 mm, 15 mm, 20 mm, 25 mm and 15 mm, respectively. The thickness of the layers was chosen to distribute the number of the interactions more equally among the segments for γ rays coming from the front and to allow the study of the effects of different thicknesses on the transient-signal (see next section) sensitivity. The Ge crystal resides in a 1 mm thick aluminium can of the same shape as the crystal. This can is separated from the crystal by 1 mm to simulate the close packed geometry of individually

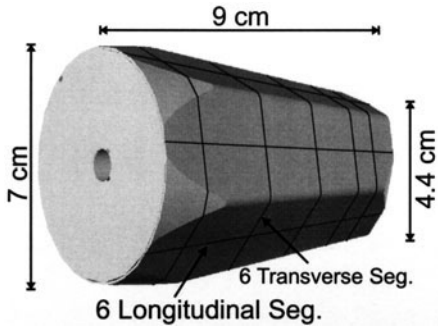

Figure 20. The 36-fold segmented GRETA prototype detector with its tapered and hexagonal shape and the arrangement of its segments.

encapsulated detectors. It is possible to mount these two-dimensionally segmented HPGe detectors in 0.7 mm thick cans with 0.7 mm gap between crystal and capsule. Such a capsule has been shown to be feasible by the MINIBALL collaboration [64] (see sections 4.4.3 and 4.5). The minimization of capsule thickness and gap size is important in order to maximize solid-angle coverage as well as add-back efficiency. To maximize the signal-to-noise ratio of the signals, the 37 FETs (36 segments + 1 central contact) of the GRETA prototype detector are located and cooled in the same vacuum as the crystal.

7.1.2. Pulse-shape analysis. Pulse-shape analysis [73] in a two-dimensionally segmented detector determines the position in three dimensions with an accuracy far better than the segmentation size. This is achieved not only by measuring the net charge signal of the charge collecting electrode but also the transient signals of neighbouring segments which display temporary image charges.

Signal measurement and calculation. In the detector, a signal (integrated current as a function of time) is produced when electrons and holes, formed by the slowing down of the photo, Compton, or pair-production electrons, induce image charges of opposite sign on the electrodes. As the charges drift toward the electrodes, the amount of the image charge changes and currents flow into or out of the electrodes. When the charge is at a large distance from the electrodes, the induced charge is distributed over several electrodes. As the charge moves closer to the destination electrode, the induced charge on this electrode increases and charges on the other electrodes decrease until the charge finally reaches the destination electrode and neutralizes the image charge. The observation of a net charge on the destination or charge-collecting electrode (segment B4 in figure 21) can be used to identify the segment which contains the interaction. In contrast, the predominant characteristic of the transient signals is that they vanish when the charge carriers are collected. In addition, either polarity is possible, depending on the positions of holes and electrons (which depend on the interaction position). For example, for an interaction sufficiently close (the exact distance depends on the geometry) to the outer electrode (e.g. $x = 22$ in figure 21), the transient signal is always negative.

Charge carrier trajectories as well as segment signals can be calculated from the electric field in the detector and the known parameterization of the charge carrier velocities as a function of electric field and crystal orientation. The field is obtained by solving the Poisson equation for the given detector geometry and boundary conditions. Transient charge signals are calculated via the so-called weighted field method.

Position sensitivity. In figure 21, measured as well as calculated segment signals are shown. The top part indicates the two locations of single-interactions in segment B4, close to the lower and front neighbours C4 and B3, respectively. The measurements were performed with the coincidence set-up shown on top of figure 22. Because of the finite size of the collimators, the signals for a given pair of collimator positions are averaged over many events in order to define a set of signals corresponding to a 'precise' interaction position, i.e. the centre of the collimated region of the detector. However, the signal noise prevents an event-by-event precise determination of the interaction position. The position sensitivity expresses the change of net and transient charge signals for different locations (determined as explained above) relative to the noise level. It measures the minimum distance between interactions that produce distinguishable signals. The obtained sensitivity of about 0.5 mm in each dimension at an energy of 374 keV (deposited in a single-interaction), is remarkable considering the fact that the size of the segment is very roughly 2 cm on each side, implying an improvement of about a factor of 40 in each dimension.

Determination of the interaction position. In order to track, an event-by-event interaction position determination is needed. It is in principle obtained by decomposing each measured signal into sets of basis of measured signals which correspond to a precise single-interaction position (obtained by averaging as explained in the previous paragraph). However, due to time constraints of data collection, it was only possible to measure basis sets of signals for a few regions of the crystal. Calculated signals corresponding to the same positions fit the data exceptionally well as shown in figures 21 and 22 and only calculations are then used to obtain sets of basis signals over the entire crystal.

Position resolution. The position resolution is the FWHM of a position spectrum obtained from a specific location in the crystal. The true position resolution has to be measured event-by-event by decomposing the measured signals with the single-interaction sets of basis signals. This gives the position distributions measured for a given collimated source position (bottom solid curves of figure 22). The width of these position distributions results from a convolution of the collimator sizes and the position resolution. The measured widths give a position resolution of 0.6–1 mm (figure 22, bottom), again at an energy of 374 keV. These distributions are well reproduced by a calculation under the same conditions (bottom dashed curves of figure 22, see caption), where a known noise has been added to the calculated signals. The displacement of the calculated curves relative to the experimental ones in the y dimension corresponds to a position deviation (centroid of the peak) of about 2 mm which is due to crystal orientation effects not taken into account in these calculations.

Multiple interactions. The real situation is more complicated and involves multiple interactions in multiple segments. For example, a 1.3 MeV γ ray, fully stopped in one crystal, interacts on average 4 times (two interactions in two segments). Several fitting procedures have been explored: conventional least-square fitting, singular value decomposition, artificial neural networks and genetic algorithms. The goal of most of the fitting procedures is to decompose the measured signals into the *a priori* calculated basis signals. To perform this decomposition calculations in real time with a sustained event rate of up to 50 kHz represents one of the remaining challenges. Current results vary in achievable position, energy-resolution and, especially, in processing times.

7.1.3. Tracking algorithms. The reconstruction of γ rays is the third major task required to realize a γ-ray tracking array. The interaction information is used by tracking algorithms [71] to separate and identify the γ rays.

Compton scattering. Figure 23 shows a world map of interactions obtained by Monte-Carlo simulations (GEANT3) for 25 γ rays with an energy of 1.33 MeV launched from the centre into an ideal Ge shell with an inner radius of 15 cm and a thickness of 9 cm. The Compton scattering process is dominant for these γ rays as well as in the region of main interest, e.g. between 150 keV and 8 MeV. One of the current Compton-tracking algorithms consists of three steps. Cluster identification is the first step. The interaction points within a given angular separation (called angle parameter) as viewed from the γ-ray source are grouped into a cluster. In the second step, each cluster is evaluated by tracking to determine whether it contains all the interaction points belonging to a single γ ray. The tracking algorithm uses the angle-energy relation of Compton scattering to determine the most likely scattering sequence from the position and energy of the interaction points. As discussed in section 6.1.1, we identify good clusters based on a small deviation χ^2 from a Compton-scattering sequence. In the third step, we try to recover some of the wrongly identified clusters. For example, one type of incorrectly identified cluster comes from a single γ ray being separated into two clusters. This γ ray can be correctly identified by tracking together all pairs of bad clusters. When the result gives a small χ^2, the γ ray is recovered by adding the two clusters. The clusters which do not satisfy any of the above criteria are rejected. Assuming a position resolution of 1 mm which appears to be feasible, an angle parameter of 8°, and 25 emitted 1.33 MeV γ rays, a peak

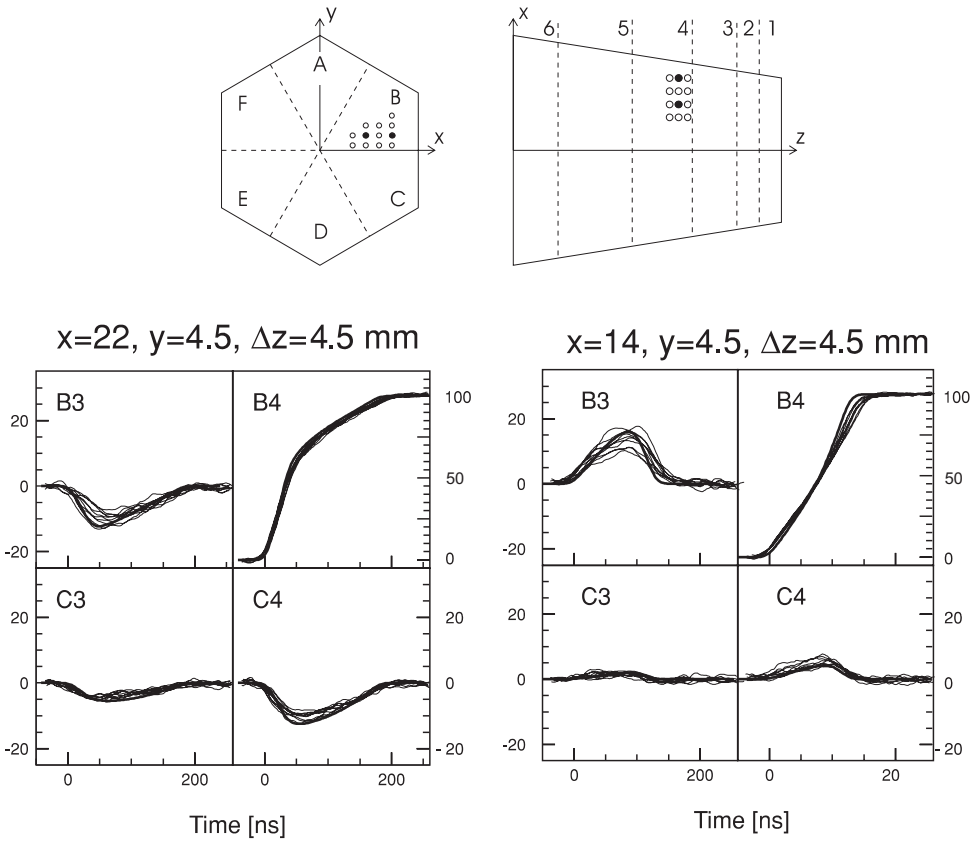

Figure 21. Measured set of segment signals at $x = 22$ mm (left) and $x = 14$ mm (right), $y = 4.5$ mm and $z = 34.5$ mm ($\Delta z = 4.5$ mm). Segment B4 contains the interactions. The thin lines are measured signals, the thick lines are calculated signals.

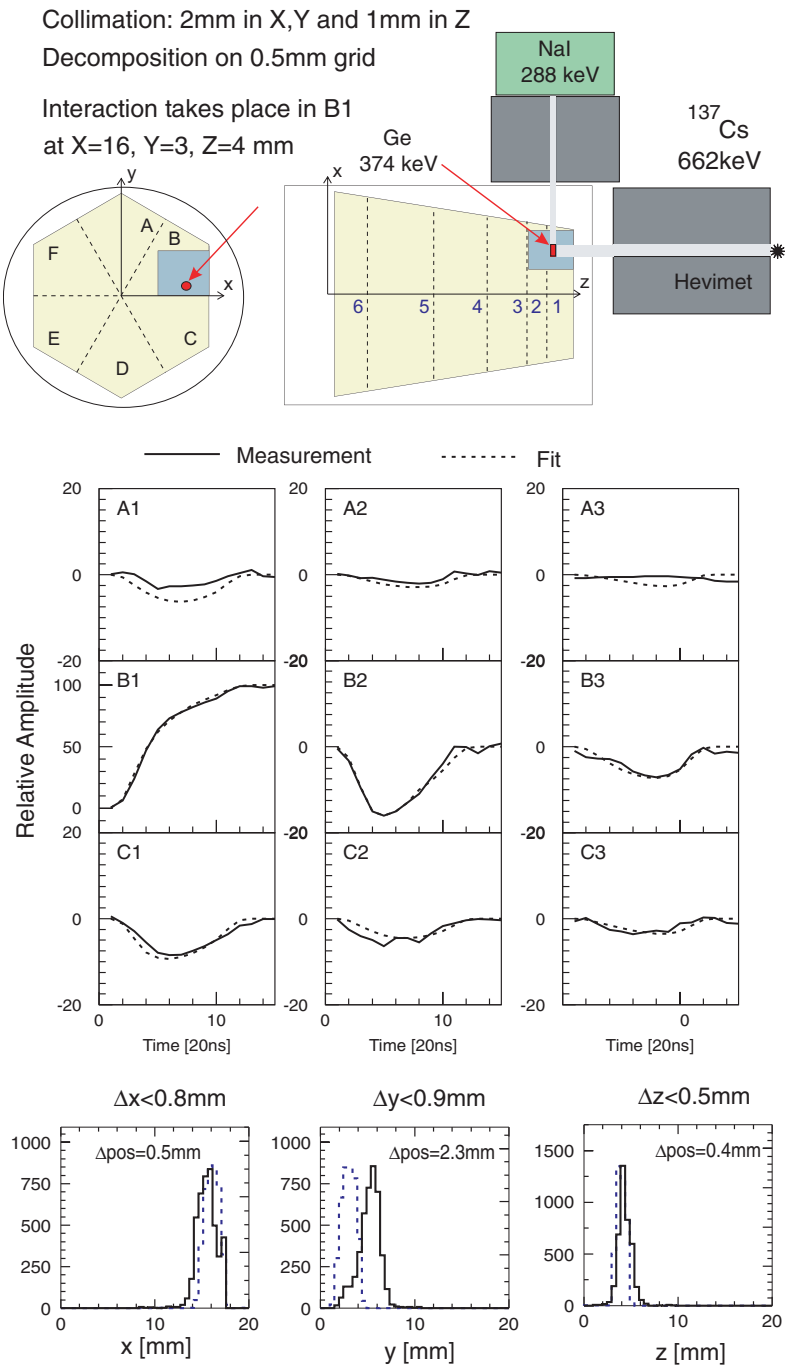

Figure 22. Top: coincidence set-up used to determine position resolution. Middle: example of calculated (- - - -) and measured (——) signals. Bottom: measured (——) and simulated (- - - -) distributions of interaction positions, x, y, and z. Deduced position resolutions Δx, Δy, Δz. Displacements of average positions, Δpos, between measurements and calculations.

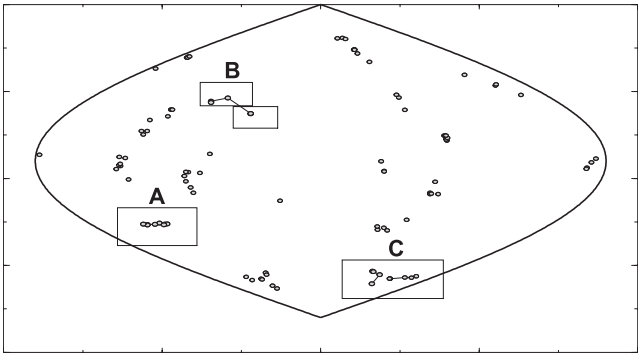

Figure 23. 'World map' of interactions obtained by launching 25 γ rays with energies of 1.33 MeV into an ideal Ge shell. 'A' shows a correctly identified cluster, 'B' shows two wrongly identified clusters which came from one γ ray and 'C' shows one wrongly identified cluster which is caused by two γ rays.

efficiency of 33% and a peak-to-total of 72% can be achieved. In comparison, Gammasphere has an efficiency of about 8% and a peak-to-total of about 50% under the same conditions, which implies a gain of four in efficiency and 1.5 in peak-to-total for each γ ray. Note that a typical high-spin event where five full-energy γ rays are recorded is then approximately $4^5 \sim 1000$ times more likely and $(1.5)^5$ times cleaner.

Pair production. At 10 MeV, the probability of pair production is about 60%. In most cases, pair production occurs at the first interaction because the energy of γ rays decreases rapidly as a Compton scattering sequence proceeds. The electron and positron pair produced by a 10-MeV γ ray have short ranges, less than 6 mm in Ge. The annihilation of the positron produces two 0.511-MeV γ rays and each of them creates a cluster of interaction points. Therefore, the pattern of pair-production events can be characterized as a single high-energy point surrounded by low-energy points. Such an algorithm was tested and a preliminary result gives a value of tracking efficiency $\varepsilon_t \sim 0.5$ at 10 MeV for an energy-resolution of 2 keV and a position resolution of 3 mm. The full-energy-peak efficiency for pair events is the product of ε_t and the full-absorption efficiency ε_a ($\sim$0.7 at 10 MeV) for the Ge shell.

Effect of neutrons. Neutrons, produced most often in nuclear reactions at energies around 1 MeV, interact primarily by elastic scattering [71]. These neutrons interact 4–5 times with the array, depositing about 5% of their energy per interaction before leaving the Ge shell. However, prompt coincidence timing eliminates the majority of neutron interactions. The remaining interactions are eliminated during the γ-ray tracking phase of the algorithm since these neutron clusters do not resemble good γ-ray clusters.

7.2. Expected performance

From the measurements on the prototype detector and from the simulations, we can infer the expected characteristic properties of GRETA.

7.2.1. Efficiency, peak-to-total ratio, position resolution, and rate. Figure 24 shows photopeak efficiencies and P/T ratios as a function of energy for GRETA and Gammasphere,

based on simulations of single γ rays without tracking. In particular, for high γ-ray energies the gain of a closed shell is very large. Efficiencies of up to 10% are expected at γ-ray energies of 10 MeV while Gammasphere provides only about 0.5% at this energy. The gain in the P/T ratio at higher γ-ray energies is also quite large and is due to the full coverage of Ge detectors which can contain the larger spatial distribution of higher energy γ rays. In Gammasphere, this larger distribution is unlikely to be contained in a single Ge detector. For higher γ-ray multiplicities, the performance for GRETA with tracking depends on the achievable position resolution and the minimal resolvable distance between two interactions. With a position resolution of 1–2 mm, figure 25 shows calculated [71] efficiencies and P/T ratios for GRETA when tracking 25 γ rays of 1.33 MeV as a function of the angle parameter. The calculated numbers for Gammasphere at this multiplicity and this energy are shown for comparison. At an angle parameter of 8° one can conservatively expect an efficiency of about 30% and a P/T ratio of 70%. In addition, we estimate that because of the shorter processing time and the increased number of segments, the event rate can be increased by a factor of about 20.

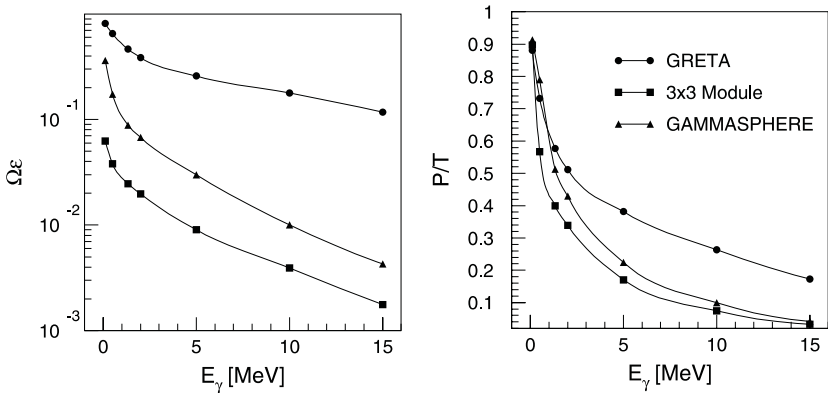

Figure 24. Calculated photopeak efficiencies (left) and P/T ratios (right) for GRETA, Gammasphere and a cluster of 3 × 3 GRETA type detectors as a function of γ ray energy for single γ rays without tracking.

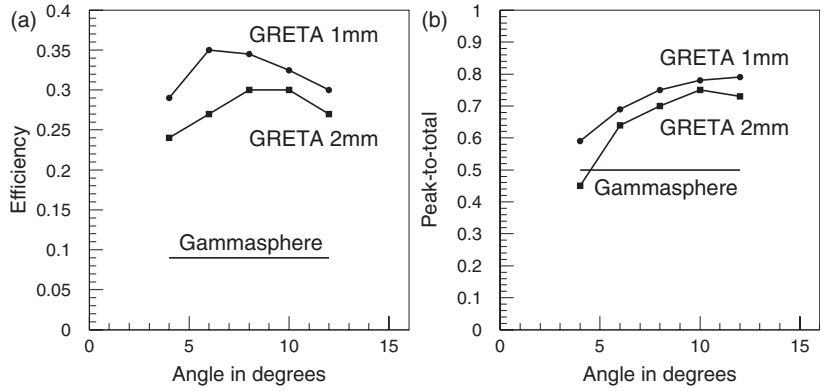

Figure 25. Calculated photopeak efficiencies and P/T ratios for GRETA after tracking, assuming 25 γ rays with 1.33 MeV.

7.2.2. Resolving power. Based on the efficiencies and the P/T ratios in figure 25 the expected resolving power of GRETA will be approximately 7×10^6, an increase in sensitivity by three orders of magnitude from Gammasphere and Euroball.

The substantial gain in sensitivity of a γ-ray tracking array is not limited to experiments with high γ-ray multiplicities. Tremendous improvements due the enhanced Doppler-shift correction capability can also be expected for high recoil-velocity events even at low γ-ray multiplicities. Also large improvements in efficiency for high γ-ray energies are expected under any conditions.

7.3. Recent developments and future plans for GRETA

The above discussion has outlined the design and expected performance of GRETA. This section will give the present status of detector- and signal analysis-development.

7.3.1. Detector prototypes and the GRETA array. Development of segmented HPGe co-axial detectors began with Gammasphere in 1993 with two segments (2×1, see section 4.4.2) and table 1 lists various types of segmented detectors used in current or planned arrays. The first GRETA prototype used a 6×2 segmentation. This detector was tested in 1997. The second prototype with 6×6 segmentation was extensively tested in 1999–2000.

The next important step towards building a full γ-ray tracking array such as GRETA is the manufacture of a cluster of three encapsulated, 6×6 segmented HPGe detectors. All three detectors will be assembled close together in one cryostat. This arrangement represents a compromise between minimizing support structure and gaps on one hand and providing adequate reliability and cooling capabilities on the other hand. Since each Ge crystal is equipped with 37 FETs, a total of 111 FETs have to be cooled down in the cryostat. The main purpose of this module is the development of the technology to assemble and operate three close-packed and highly segmented HPGe detectors in one cryostat. The first cluster was ordered in the fall of 2002 with delivery expected in the fall of 2003. If successful, two more clusters will be acquired. This small array of 9 Ge detectors [78] (see figure 26) will test γ-ray tracking across cryostat boundaries. A photopeak efficiency of up to 3% and a P/T ratio of about 50% at 1.33 MeV can be expected using tracking in this 3×3 GRETA cluster (see figure 24).

7.3.2. Signal digitizer and signal processing. Recent technological advances of fast-sampling and high-resolution ADCs and the evolution in processing speed provide the required pulse-shape analysis and tracking capabilities to process the large amount of complex data in real time.

Planned waveform digitizer systems consist of 12 or 14 bit ADCs with a sampling rate of 100 MHz. While the signal decomposition calculations can be run in parallel for each individual detector, the tracking calculations have to be performed with information from all detectors. However, the event stream can be parallelized again over a network of processing units. In a high γ-ray multiplicity experiment, current signal decomposition calculations will require in the order of 15 Gops s^{-1} per crystal. In such an experiment, the tracking alone will require about 1 Tops s^{-1}.

Presently, an 8-channel, 12-bit, 100 MHz flash-ADC board has been produced at LBNL and is being tested. It includes a set of leading-edge discriminators, constant fraction discriminators, an energy algorithm and a user adjustable window to extract relevant parts of pulse-shape for subsequent signal decomposition. The VME readout of the board is designed for a sustained counting rate of 10 000 counts s^{-1}.

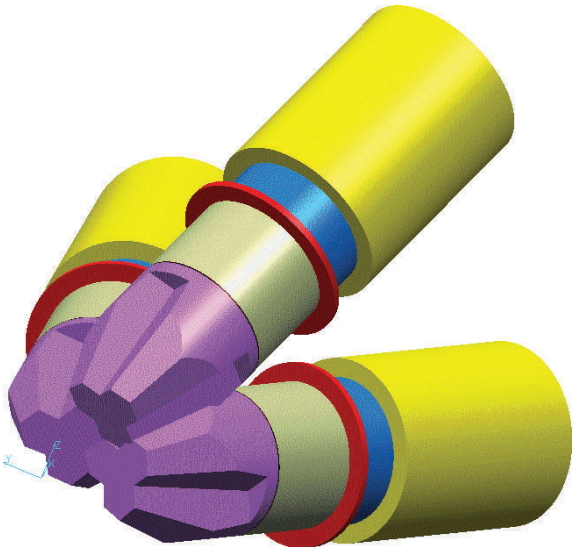

Figure 26. Design of a group of three clusters, each consisting of three encapsulated, 6 × 6 segmented detectors.

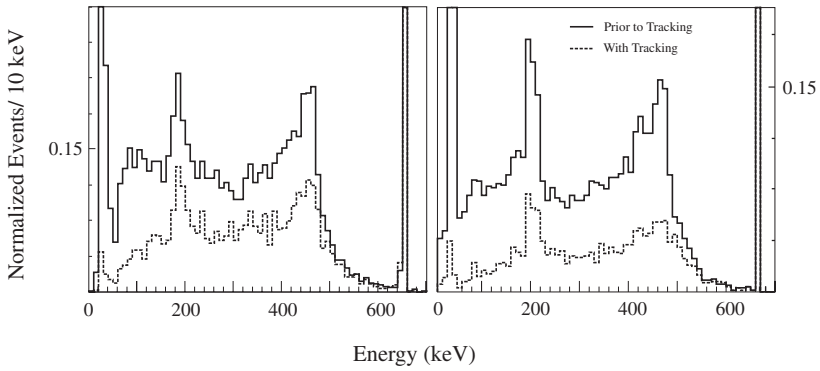

Figure 27. Measured (left) and calculated (right) energy spectra from ^{137}Cs with 662 keV. The solid lines show the raw spectra without tracking, and the dashed lines show the spectra with tracking. All spectra are normalized to the intensity of the 662 keV full-energy line, which is off-scale.

7.3.3. Determination of double hits in a segment. The signal decomposition procedure translates measured signal shapes into number of interactions, energies and positions. Based on the simulation calculations, the currently employed general least square minimization procedure, which is subject to both linear and non-linear constraints on the fit parameters, is able to separate single from double interactions in a segment in 70–90% of all cases at an energy of 662 keV.

7.3.4. Full analysis of simulated and measured data. Comparisons have been made of measured spectra with purely simulated spectra both prior to the decomposition and tracking procedure and afterward. This determines the effect of tracking in efficiency and P/T ratio for the 36-fold segmented GRETA prototype detector. Figure 27 illustrates the gain in P/T ratio

by tracking in the GRETA prototype detector [79]. On the left, the measured raw spectrum is shown together with the spectrum obtained after tracking. On the right, figure 27 shows a spectrum which was generated by Monte-Carlo simulations and calculated signals (solid line). The simulations provide positions and energies of individual interactions which are used to calculate signals from each segment. To make the signal more realistic, detector and preamplifier response as well as previously measured noise levels were folded into the signals. From there, the same tracking procedure as used for the measured data was employed (dashed line). In both figures, spectra have been normalized to the initial full-energy line at 662 keV.

In the measured data the P/T ratio was improved from 0.16 to 0.31 with tracking, and the photopeak efficiency dropped to 0.62. For the calculated spectra shown on the right of figure 27, a gain in the P/T ratio from 0.22 to 0.47 was obtained with tracking and the efficiency decreased to 0.67, a value similar to the real data. The overall low values of the P/T ratios of 0.16 or 0.22 are due to several non-functioning segments which complicate the measurement. The lower value of the measured as compared with the calculated P/T value is due the difficulty in parameterizing the environment of the detector accurately. However, both values scale very similarly with the application of tracking.

While the performance in terms of P/T ratio and efficiency for single γ-ray tracking is inferior to that of a Compton-suppressed detector, the performance improves quickly for more detectors where scattered γ rays can be tracked across detector boundaries. This can be seen in figure 24 where the expected performance of the 3×3 cluster is shown.

7.4. GRETA capabilities for new physics

The main improvement brought by the first- and second-generation arrays was a large increase in sensitivity or resolving power over the previous systems which consisted of only a few detectors. GRETA not only has a resolving power increased by a factor close to 1000 over second-generation arrays but also provides entirely new capabilities brought about by the possibility of tracking.

7.4.1. GRETA with the ISOL-type radioactive beams. The scattering angle between the first two interactions defines the angle of the incident γ ray. In experiments with radioactive beams, tracking can determine whether γ rays come from the target or from unwanted residual activity in the target chamber due to the radioactive beam itself. This capability will enormously increase the sensitivity of radioactive beam experiments and will considerably extend the range of exotic nuclei that can be studied.

The location of the first and second interaction provides the linear polarization of the incident photon. In GRETA, the polarization sensitivity is increased by a factor of at least 100 compared with Gammasphere or Euroball. This will help determine the spins and parities in many exotic nuclei and will also have implications in nuclear astrophysics.

7.4.2. GRETA with fragmentation-type radioactive beams. Through tracking, we can locate the first interaction of a γ ray within 1–2 mm anywhere in the γ-ray detector. For the most dramatic case of a high-velocity γ-emitting nucleus ($v/c \sim 30\%$) the Doppler broadening in a GRETA detector located at 90° to the nuclear velocity would be 10 times smaller than with a Gammasphere detector at a similar location. This is essential for experiments with radioactive beams obtained by the fragmentation method and makes possible studies of the collective modes and nuclear shapes in many very exotic nuclei.

7.4.3. GRETA for high-energy γ rays. GRETA will be approximately 20 times more efficient than Gammasphere for a 10 MeV γ ray. Here, the combination of high efficiency and high energy-resolution is unprecedented. For example, the elusive giant dipole resonance built on SD states is likely to be found and studied, yielding more detail on the collective properties of SD nuclei. The combination of tracking and high efficiency will also permit the study of giant resonances in very exotic nuclei.

7.4.4. GRETA for studies of high-angular-momentum states. Figure 28 illustrates the gains in resolving power achieved over the years for the various detectors considered in this review. The gain was considerable with the construction of HPGe detector arrays, but GRETA will achieve an even bigger step. The bottom left part of the figure shows that γ rays of correspondingly lower intensity, coming from higher and higher nuclear spins states, could be observed, with

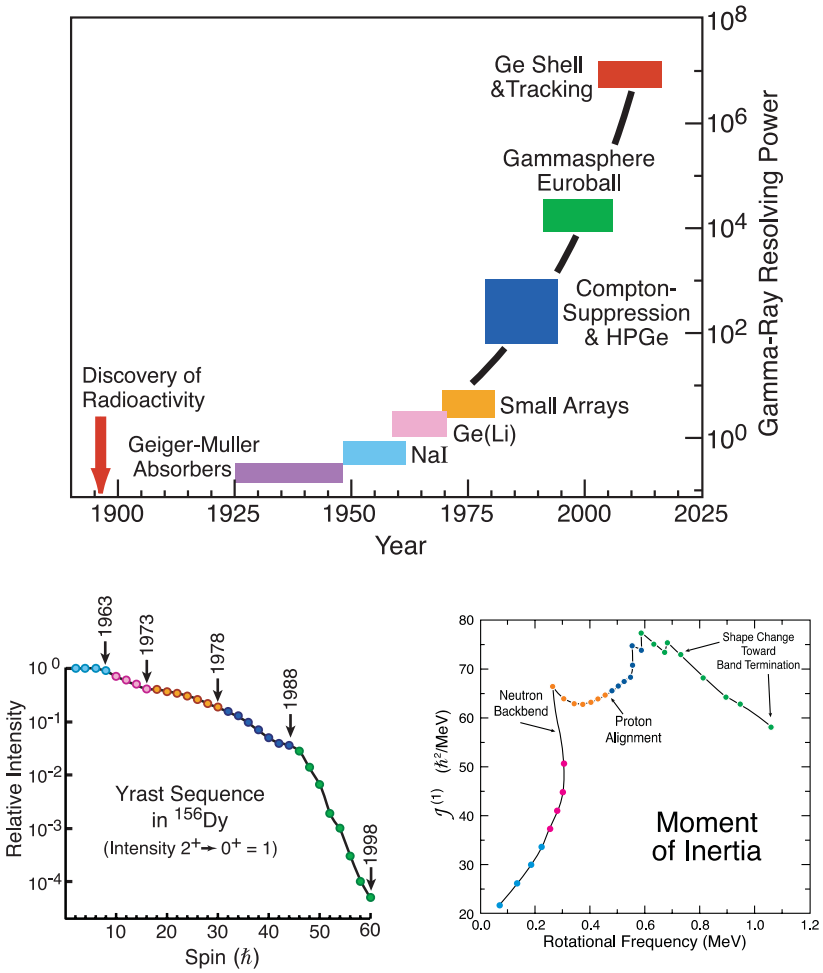

Figure 28. Top: the evolution of the resolving power for various detectors and detector arrays including the prediction for Ge shells such as GRETA. Bottom: (left) relative intensity of the yrast sequence in ^{156}Dy as a function of spin; the arrows mark the location of the highest spin observed at the dates indicated; (right) moments of inertia of the yrast sequence in ^{156}Dy as a function of the rotational frequency; various phenomena corresponding to 'kinks' in the curve are indicated.

the spin 60 corresponding to the limit from Gammasphere and Euroball. The bottom right part shows that new nuclear properties were discovered as the observable frequency of the rotating nucleus was increased (a rotational frequency of ∼1 MeV corresponds roughly to the spin ∼60$\hbar$ in the left part of the figure). With GRETA it should be possible to investigate very weak transitions and address such topics as: the systematic study of the decay between SD and ND states; the search for nuclei with even more elongated, 'hyperdeformed', shapes (with a ratio of axes ∼3 : 1), expected to occur at very high spins (70–80$\hbar$); the investigation of nuclear structure at increasing temperature where new phenomena associated with the evolution from order to chaos occur.

7.4.5. Other science. Other branches of physics would also benefit from the power of GRETA. For example, the study of the positronium decay into four or five photons would provide higher order tests of quantum electrodynamics and improve limits on charge conjugation symmetry violating currents. In particle physics, measurements of the V_{ud} element of the quark mixing matrix, important for tests of the Standard Model, could be improved by a factor of ∼10 in the most important case of ^{10}C by distinguishing between a 1022 keV γ ray and the sum of two 511 keV γ rays. In astrophysics, so-called Compton cameras to image the distant sky will be improved by event-by-event tracking of the first and second interactions to determine the incoming γ-ray direction. Efficient imaging of radioactive sources through tracking will have important applications in other areas of science. For example, in medicine, a new class of radioisotopes with multiple γ rays could be used. In safeguarding against terrorism, higher energy γ rays, more difficult to shield, can be used to find hidden materials.

8. Conclusion

The development of γ-ray detectors and of arrays has played a very important role in scientific discoveries. Arguably, the most important milestones have been the development of NaI(Tl) detectors, then Ge detectors, and recently large arrays of BGO Compton-suppressed HPGe detectors. In each case, pressing new physics questions motivated the quest for detector improvements, and new technologies made possible these new designs. In the last two sections, we have tried to show that γ-ray tracking is a new technique, requiring entirely new highly segmented Ge detectors, and new kinds of data handling (digital signal processing and tracking). We have reviewed the detector developments and focused on the progress made in nuclear spectroscopy. However, tracking techniques will benefit many areas of science and a major effort to develop them is presently underway worldwide.

Acknowledgments

The authors would like to thank F S Stephens, R M Clark and A O Macchiavelli for critical reading of the manuscript and for useful suggestions. This work was supported by the Director, Office of Energy Research, Division of Nuclear Physics of the Office of High Energy and Nuclear Physics of the US Department of Energy under contract No DE-AC03-76SF00098 and under the auspices of the US Department of Energy by University of California Lawrence Livermore National Laboratory under contract No W-7405-Eng-48.

References

[1] Deleplanque M A and Diamond R M (ed) 1987 Gammasphere proposal *Preprint* LBNL-5202
[2] Siegbahn K 1965 *Alpha-, Beta- and Gamma-Ray Spectroscopy* (Amsterdam: North-Holland)

[3] Evans R D 1955 *The Atomic Nucleus* (New York: McGraw-Hill)
[4] Klein O and Nishina Y 1929 *Z. Phys.* **52** 853–68
[5] Knoll G F 2000 *Radiation Detection and Measurement* (New York: Wiley)
[6] Tavendale A J and Ewan G T 1963 *Nucl. Instrum. Methods* **25** 125–87
[7] Goulding F S 1966 *Nucl. Instrum. Methods* **43** 1–54
[8] Haller E E 1982 *IEEE Trans. Nucl. Sci.* **NS-29** 1109–18
[9] Pell E M 1960 *J. Appl. Phys.* **31** 291–302
[10] Hall R N and Soltys T J 1971 *IEEE Trans. Nucl. Sci.* **NS-18** 160–5
[11] Hansen W L 1971 *Nucl. Instrum. Methods* **94** 377–80
[12] Beausang C W and Simpson J 1996 *J. Phys. G: Nucl. Particle Phys.* **22** 527–58
[13] Simpson J 1997 *Z. Phys.* A **358** 139–43
[14] Hull E 1998 Charge collection physics in germanium detectors *PhD Thesis* Indiana University
[15] Pehl R H 1977 Germanium gamma-ray detectors *Phys. Today* November 50–61
[16] Pehl R H *et al* 1979 *IEEE Trans. Nucl. Sci.* **NS-26** 321–3
[17] Raudorf T W, Trammell R C, Wagner S and Pehl R H 1984 *IEEE Trans. Nucl. Sci.* **NS-31** 253–7
[18] Pehl R H *et al* 1968 *Nucl. Instrum. Methods* **59** 45–55
[19] Goulding F S and Landis D A 1982 *IEEE Trans. Nucl. Sci.* **NS-29** 1125–41
[20] Radecka V 1964 *IEEE Trans. Nucl. Sci.* **NS-11/3** 358–64
[21] Van der Ziel A 1962 *Proc. IRE* **50** 1808–12
[22] American National Standards Institute 1991 ANSI N42.14-1991
[23] Luke P N *et al* 2001 *Nucl. Instrum. Methods Phys. Res.* A **458** 319–24
[24] Jäskeläinen M *et al* 1983 *Nucl. Instrum. Methods* **204** 385–405
[25] Habs D, Stephens F S and Diamond R M 1979 A proposal for a crystal-ball detector system *Preprint* LBL-8945, pp 1–68
[26] Simon R S 1980 *J. Phys.* **41 C10** 281–93
[27] Stephens F S 1988 Private communication
[28] Deleplanque M A *et al* 1999 *Nucl. Instrum. Methods* A **430** 292–310
[29] Twin P J 1981 *Workshop on Nuclear Structure at High Spin (Risø, Denmark)* pp 135–6, unpublished
[30] Twin P J 1984 *Proc. Conf. on Instrum. for Heavy Ion Nuclear Research Nucl. Sci.* Research Conf. Series vol 7 ed Schapira D Harwood, pp 231–57
[31] Sharpey-Schafer J F and Simpson J 1988 *Prog. Particle Nucl. Phys.* **21** 293–400
[32] Diamond R M and Stephens F S A 1981 Proposal for the high resolution ball, LBNL, unpublished
[33] Diamond R M 1984 *Proc. Conf. on Instrum. for Heavy Ion Nucl. Res. Nucl. Sci.* Research Conf. Series vol 7 ed Schapira D Harwood, pp 259–81
[34] Lieder R *et al* 1984 *Nucl. Instrum. Methods* **220** 363–70
[35] Martin J P *et al* 1987 *Nucl. Instrum. Methods* A **257** 301–08
[36] Herskind B *et al* 1985 *Nucl. Phys.* A **447** 395c–412c
[37] Beck F A 1984 *Proc. Conf. on Instrum. for Heavy Ion Nuclear Research Nucl. Sci.* Research Conf. Series vol 7 ed Schapira D Harwood, pp 129–45
[38] Twin P J 1986 *Phys. Rev. Lett.* **57** 811–14
[39] Bazzaco D 1992 *Proc. Workshop on Large γ-ray Detector Arrays (Chalk River Canada)* AECL-10613, pp 376–82
[40] Beausang C W *et al* 1992 *Nucl. Instrum. Methods* A **313** 37–49
[41] Pugh A 1976 *Polyhedra: A Visual Approach* (Berkeley, CA: University of California Press)
[42] Baxter A M *et al* 1992 *Nucl. Instrum. Methods* A **317** 101–10
[43] Carpenter M P *et al* 1994 *Nucl. Instrum. Methods* A **353** 234–8
[44] Macchiavelli A O *et al* 1994 *Proc. Conf. on Physics from Large γ-ray Detector Arrays (Berkeley)* LBL 35687 CONF 940888 UC413, pp 149–53
[45] Sarantites D G *et al* 1996 *Nucl. Instrum. Methods* A **381** 418–32
[46] Sarantites D G 1999 WWW at http://wunmr.wustl.edu/ dgs/NeutronShell
[47] Simon M W *et al* 2000 *Nucl. Instrum. Methods* A **452** 205–22
[48] Davids C N 1992 *Nucl. Instrum. Methods* B **70** 358–65
[49] Beck F A *et al* 1994 *Proc. Conf. on Physics from Large γ-ray Detector Arrays (Berkeley)* LBL 35687 CONF 940888 UC413, pp 154–8
[50] Duchene G *et al* 1999 *Nucl. Instrum. Methods* A **432** 90–110
[51] Eberth J *et al* 1996 *Nucl. Instrum. Methods* A **369** 135–40
[52] Eberth J 1992 *Prog. Particle Nucl. Phys.* **28** 495–504

[53] Eberth J 1994 *Proc. Conf. on Physics from Large γ-Ray Detector Arrays (Berkeley)* LBL 35687 CONF 940888 UC413, pp 160–4
[54] Eberth J *et al* 1997 *Prog. Particle Nucl. Phys.* **38** 29–37
[55] Euroball website at http://eballwww.in2p3.fr
[56] Khoo T L 1996 *Phys. Rev. Lett.* **76** 1583–6
[57] Lopez-Martens A *et al* 1996 *Phys. Lett.* B **380** 18–23
[58] Hauschild K *et al* 1997 *Phys. Rev.* C **55** 2819–25
[59] Lauritsen T 2002 *Phys. Rev. Lett.* **88** 042501–4
[60] Simpson J *et al* 2000 *APH N.S. Heavy Ion Phys.* **11** 159–88
[61] Azaiez F 1999 *Nucl. Phys.* A **654** 1003c–8c
[62] Svensson C E *et al* 2003 *Proc. Int. conf. on Electromagnetic Isotope Separators and Their Applications (Victoria Canada) Nucl. Instrum. Methods* B, ed J d'Auria, at press
[63] Habs D *et al* 1997 *Prog. Particle Nucl. Phys.* **38** 111–26
[64] Eberth J *et al* 2001 *Prog. Particle Nucl. Phys.* **46** 389–98
[65] Mueller W F *et al* 2001 *Nucl. Instrum. Methods* A **466** 492–8
Glasmacher T 2002 website at http://www.nscl.msu.edu
[66] Goulding F S 1972 *Nucl. Instrum. Methods* **100** 493–504
[67] Gobbur S G, Landis D A and Goulding F S 1977 *Nucl. Instrum. Methods* **140** 405–6
[68] Cottini C, Gatti E and Svelto V 1963 *Nucl. Instrum. Methods* **24** 241–2
[69] Mc-Pherson G M *et al* 1992 *IEEE Trans. Nucl. Sci.* **39** 886–91
[70] Lazarus I and Coleman-Smith P 1995 *IEEE Trans. Nucl. Sci.* **42** 891–4
[71] Schmid G J *et al* 1999 *Nucl. Instrum. Methods* A **430** 69–83
[72] Vetter K *et al* 2000 *Nucl. Instrum. Methods* A **452** 105–14
[73] Vetter K *et al* 2000 *Nucl. Instrum. Methods* A **452** 223–38
[74] 2003 http://www.cordis.lu/tmr/home.html
[75] 2002 http://www.lnl.infn.it
[76] 2002 http://www-gsi-vms.gsi.de/eb/html/agata.htm
[77] Lister C J and Phlips B 2000 Slide report from the *TMR User Meeting on Gamma-ray Tracking Detectors (Cologne Germany)* ed J Eberth and R M Lieder
[78] 2000 Proposal for a GRETA Module Cluster LBNL
[79] Kuhn A L 2002 Advanced pulse-shape analysis and implementation of gamma-ray tracking in a position-sensitive coaxial HPGe Detector *PhD Thesis* University of California Berkeley